

## Global empirical model of TEC response to geomagnetic activity

P. Mukhtarov,<sup>1</sup> B. Andonov,<sup>1</sup> and D. Pancheva<sup>1</sup>

Received 9 March 2013; revised 4 August 2013; accepted 16 September 2013.

[1] A global total electron content (TEC) model response to geomagnetic activity described by the  $K_p$  index is built by using the Center for Orbit Determination of Europe (CODE) TEC data for a full 13 years, January 1999 to December 2011. The model describes the most probable spatial distribution and temporal variability of the geomagnetically forced TEC anomalies assuming that these anomalies at a given modified dip latitude depend mainly on the  $K_p$  index, local time (LT), and longitude. The geomagnetic anomalies are expressed by the relative deviation of TEC from its 15 day median and are denoted as rTEC. The rTEC response to the geomagnetic activity is presented by a sum of two responses with different time delay constants and different signs of the cross-correlation function. It has been found that the mean dependence of rTEC on  $K_p$  index can be expressed by a cubic function. The LT dependence of rTEC is described by Fourier time series which includes the contribution of four diurnal components with periods 24, 12, 8, and 6 h. The rTEC dependence on longitude is presented by Fourier series which includes the contribution of zonal waves with zonal wave numbers up to 6. In order to demonstrate how the model is able to reproduce the rTEC response to geomagnetic activity, three geomagnetic storms at different seasons and solar activity conditions are presented. The model residuals clearly reveal two types of the model deviation from the data: some underestimation of the largest TEC response to the geomagnetic activity and randomly distributed errors which are the data noise or anomalies generated by other sources. The presented TEC model fits to the CODE TEC input data with small negative bias of  $-0.204$ , root mean squares error RMSE = 4.592, and standard deviation error STDE = 4.588. The model offers TEC maps which depend on geographic coordinates ( $5^\circ \times 5^\circ$  in latitude and longitude) and universal time (UT) at given geomagnetic activity and day of the year. It could be used for both science and possible service (nowcasting and short-term prediction); for the latter, a detailed validation of the model at different geophysical conditions has to be performed in order to clarify the model predicting quality.

**Citation:** Mukhtarov, P., B. Andonov, and D. Pancheva (2013), Global empirical model of TEC response to geomagnetic activity, *J. Geophys. Res. Space Physics*, 118, doi:10.1002/jgra.50576.

### 1. Introduction

[2] The ionosphere, where the free electrons are formed mainly by the solar X-rays and EUV radiation, is above all under solar control but is dependent also on various chemical and dynamical processes with thermosphere, magnetosphere, and lower atmosphere. Usually during periods of high solar activity through the interaction between coronal mass ejections and the Earth's magnetic field, large geomagnetic disturbances are excited. Such disturbances can lead to a significant perturbation of the “quiet time” ionosphere due to large variability in the ionospheric density distribution, total electron content (TEC), and the ionospheric current

system. The rapid and global response of the ionosphere to these strong geomagnetic disturbances is well studied [Mendillo *et al.*, 1970, 1974, 1992; Prölss, 1980, 1991, 1993, 1995, 2008; Rishbeth, 1991, 1998; Field and Rishbeth, 1997; Fuller-Rowell *et al.*, 1994, 1996, 2000; Muhtarov and Kutiev, 1998; Buonsanto, 1999; Kutiev and Muhtarov, 2001, 2003; Mendillo, 1973, 2006]. Three dominant causes of storm effects have been suggested to explain the positive and negative phases of ionospheric storms: thermospheric composition changes, neutral wind perturbations, and the appearance of electric fields of magnetospheric origin [Mendillo, 2006]. Satellite neutral mass spectrometer measurements showed that the negative phase of ionospheric storms is mainly due to the composition changes [Prölss, 1980, 1995, 2011], while the positive phase is caused by disturbed thermospheric wind and electric fields [Tanaka, 1979, 1981].

[3] The geomagnetic storms can have significant, adverse effects on ground- and space-based technological systems. Some important terrestrial consequences include possible damage to satellites caused by high-energy particles, disrupting

<sup>1</sup>National Institute of Geophysics, Geodesy and Geography, Bulgarian Academy of Sciences, Sofia, Bulgaria.

Corresponding author: D. Pancheva, National Institute of Geophysics, Geodesy and Geography, Bulgarian Academy of Sciences, Acad. G. Bonchev St., Block 3, 113 Sofia, Bulgaria. (dpancheva@geophys.bas.bg)

UHF satellite communications or detection and tracking of aircrafts, missiles, and other targets; increased risk of radiation exposure by humans in space and in high-altitude aircraft; changes in atmospheric drag on satellites; errors in Global Positioning System (GPS) and in VLF navigation systems; and loss of HF communications. Because the GPS signals are used by a wide range of applications, any geomagnetic storm event which makes GPS signal unreliable could have significant impact on society. Hence, the monitoring of ionosphere, particularly during the geomagnetic storms, and modeling and forecasting the evolution of the ionospheric variability are among the important tasks of the ionosphere studies.

[4] The development of the Global Navigation Satellite System (GNSS) during the last decade has provided a number of possibilities for studying the spatial distribution and temporal evolution of ionospheric electron density disturbances forced by external or internal sources. The TEC has received a great deal of attention recently because it is a key parameter related to the phase delay effects on the GNSS signals. The accurate measurement of the phase delay is a strong requirement for the reliable performance of GNSS positioning, timing, and navigation. The necessity of the data corrections obtained from the navigation satellites imposes the requirement of not only the regular variability of the electron density but also the variability related to the geomagnetic storms or other drivers to be taken in mind [Jakowski *et al.*, 2005]. As the ionosphere is the largest error source, part of these errors, particularly those related to the dispersive properties of the ionosphere (so called first-order range error), can be eliminated by using differential measurements in dual frequency systems like GPS, 1575.42 MHz at L1 and 1227.60 MHz at L2. In this case, however, the ray paths and TEC are assumed to be the same for both frequencies. During some severe geomagnetic storms, however, the polar ionosphere can be pushed  $10^\circ$  to  $30^\circ$  of latitude toward the equator and can cause large horizontal gradients of the electron density which violate the assumption for the same ray paths and TEC [Kashcheyev *et al.*, 2012]. Then, especially at high solar activity, in order to ensure precise GNSS applications, higher-order ionospheric term errors have to be considered and taken into account [Hoque and Jakowski, 2007; Elmas *et al.*, 2011].

[5] The recent investigations of the TEC response to the geomagnetic storms based on the GPS measurements obtained from the global and regional networks of International GNSS Service (IGS) ground receivers have reported the main features of the TEC response [Mendillo, 2006]. The GPS technique has great advantage in producing real-time global and regional ionosphere maps. This has provided opportunity for space physics to change from discovery mode to mainly application mode activities by building TEC empirical models for prediction. It was mentioned by Mendillo [2006] that “modeling of the TEC parameter during storms has not been extensive, and thus an emphasis on model improvements tailored for TEC is a crucial need.” Zhao *et al.* [2007] presented the latitude/longitude distribution of the relative deviation of the TEC (rTEC) during winter, summer, and equinoxes, as well as the effect of the LT. Habarulema *et al.* [2007, 2010, 2011] built regional GPS-based TEC models over Southern Africa by using a neural network analysis method. Afraimovich *et al.* [2009] investigated

the dependence of the TEC variability on the  $K_p$  index for the Northern Hemisphere (NH). The authors obtained linear regressions of the dependence of the relative TEC deviation (rTEC) on the  $K_p$  index. Only the positive dependences between the rTEC and  $K_p$  index were found for the considered latitude range; the response at high latitudes ( $50$ – $80^\circ\text{N}$ ) was stronger than that at low latitudes. Stankov *et al.* [2001, 2004] presented a correlation method for the prediction of TEC depending on the geomagnetic activity for the geographic region ( $20^\circ\text{W}$ – $40^\circ\text{E}$ ,  $32.5^\circ\text{N}$ – $70^\circ\text{N}$ ) where a time delay constant of  $\sim 18$  h and a periodic Fourier function accounted for the LT effect were introduced. Recently, Stankov *et al.* [2010] have applied a common epoch analysis on TEC data representing nearly 300 storm events from the last solar cycle. It was found that the storm time behavior of TEC shows clear positive and negative phases with amplitudes that tend to increase during the more intense storms.

[6] The TEC response to the geomagnetic activity for the American sector was reported by Araujo-Pradere *et al.* [2006]. The authors found consistent features from storm to storm, and these features became more apparent when the data were separated between the “driven” phase of the storm, when the integral of  $ap$  index is rising, and the “recovery” to the storm, when the integral of  $ap$  index is declining. Recently, Andonov *et al.* [2011] have also presented an empirical TEC model response to the geomagnetic activity for the American sector particularly valid for low solar activity. It was based on the two-dimensional (2-D) cross-correlation analysis which revealed both positive and negative phases of response. Both phases of the ionospheric response have different duration and time delay with respect to the geomagnetic activity, season, and geographical latitude. The seasonal dependence of the TEC response to geomagnetic storms is characterized by predominantly positive response in winter with a short (usually  $\sim 5$ – $6$  h) time delay while mainly negative response in summer with a long (longer than 15 h) time delay.

[7] The above report shows that only regional empirical TEC model responses to geomagnetic activity have been constructed for the time being. Due to this fact, a basic aim of the present paper is to establish a global empirical TEC model response to the geomagnetic activity described by the  $K_p$  index. This global response has to be described as a function of the calendar month, geographic latitude, longitude, and LT. The main advantage of the empirical models is that their analytical expressions are fitted to the data, so there is no systematic deviation (offset) between the model and data. The main problem, however, is how well their analytical expressions describe the observed variations. The model approach in the present study is similar to that shown in Andonov *et al.* [2011]. The TEC model is built on the long-term TEC data, January 1999 to December 2011 (13 years), from the Center for Orbit Determination of Europe (CODE) [Schaer, 1999]. The same data have been used for establishing the global background TEC model; its description and statistical evaluation are presented in Mukhtarov *et al.* [2013a, 2013b].

## 2. TEC Data Set

[8] The ionospheric TEC is derived by mapping the slant path delay of the signal from dual frequency L1 and L2 bands

observed by the global networks of IGS ground receivers [Ge *et al.*, 2004; Dow *et al.*, 2009]. IGS provides the highest precision of GPS satellite orbits and precise positions (5 mm) for 350 worldwide reference stations [Ercha *et al.*, 2012]. Usually the single ionospheric layer assumption is considered to convert the slant path TEC to vertical TEC with a mapping function. Currently, five analysis centers routinely provide global ionosphere maps (GIMs) of vertical TEC using the growing global network of dual frequency GNSS receivers [Ercha *et al.*, 2012]. These are CODE [Schaer, 1999], Jet Propulsion Laboratory (JPL) [Ho *et al.*, 1996], European Space Agency (ESA) [Feltens and Schaer, 1998; Feltens, 2007], Polytechnical University of Catalonia (UPC) [Hernández-Pajares *et al.*, 1997], and the Energy Mines and Resources Canada [Gao *et al.*, 1994]. The present TEC model is constructed on the basis of vertical TEC maps generated by the CODE center at Astronomical and Physical Institutes of the University of Bern, Switzerland ([http://cmslive3.unibe.ch/unibe/philnat/aiub/content/e15/e59/e126/e440/e447/index\\_eng.html](http://cmslive3.unibe.ch/unibe/philnat/aiub/content/e15/e59/e126/e440/e447/index_eng.html)). We particularly note that, in this paper, TEC everywhere means vertical TEC. For the current study we used data for a full 13 years, 1 January 1999 to 31 December 2011, provided from the CODE FTP directory: <ftp://ftp.unibe.ch/aiub/CODE/>. At CODE, the TEC is modeled with a spherical harmonic expansion up to degree of order 15 referring to a solar-geomagnetic reference frame [Schaer, 1999]. The 2-hourly sets are derived from GPS data of the global IGS network of about 200 stations. The GIM/CODE is regarded as one of the precise TEC maps generated from GNSS observations. The used global IGS TEC data have a time resolution of 2 h and a grid spacing of  $5^\circ \times 2.5^\circ$  in longitude and latitude, respectively, with errors of several TEC units (TECU,  $1 \text{ TECU} = 10^{16} \text{ el/m}^2$ ) [Hernández-Pajares *et al.*, 2009]. The errors of the GIMs presented by the analysis centers CODE, ESA, JPL, and UPC are determined by comparing with an independent source of TEC. The reference TEC values are provided by dual frequency altimeters on board TOPEX and JASON satellites for a period of time between 2002 and 2007. Because the altimeters are working over oceans, this comparison is considered as a pessimistic determination of the global TEC map actual errors. The main statistics of the difference TOPEX/JASON TEC-GNSS TEC, presented in Hernández-Pajares *et al.* [2009, Table 1], revealed similar results; particularly for the GIM/CODE: the bias is 1.45 TECU, the standard deviation is 5.14 TECU, and the root mean squares error is 5.35 TECU. Jee *et al.* [2010] performed a comprehensive comparison especially between the CODE GIM and TOPEX/JASON TEC data for the period of time between March 1998 and May 2009, which is directed particularly to ionospheric studies during different geophysical conditions (local time, latitude/longitude, season, and solar activity). It was found that on the whole, the GIM model was largely able to reproduce the spatial and temporal variations of the global ionosphere as well as the seasonal variations such as the annual and semiannual anomalies for all solar activities. It was noted there that the GIM model was not accurate enough to represent some ionospheric structures as the Weddell Sea Anomaly (WSA particularly during equinoxes), the longitudinal wave number 4 and 3 structures, etc. A fundamental limitation of the GIM/CODE model is detected in the northern high latitude and the southern middle- and high-latitude

regions, which are mostly occupied by oceans and include very sparse GPS ground stations. In these regions the CODE TEC values are smaller than those of the TOPEX/JASON TEC as sometimes the difference could reach 50%.

[9] The original global TEC data were arrayed in terms of the coordinate system of geographical latitude (from  $-87.5^\circ$  to  $87.5^\circ$  at each  $2.5^\circ$ ) and longitude (from  $-180^\circ$  to  $180^\circ$  at each  $5^\circ$ ). It is known, however, that the neutral wind and electric field effects on the ionosphere are dependent on the geomagnetic field configuration as the electrons are constrained to the magnetic field lines. That is why the distribution of the ionospheric parameters, including TEC as well, is usually presented in geomagnetic latitude instead of geographic one. Early investigations (reported, e.g., in Rawer [1984]) demonstrated the benefit of using the modified dip latitude (modip), introduced by Rawer [1963], to describe the variability of the densest part of the ionosphere, particularly at middle and low latitudes. The modified dip (modip) latitude which is adapted to the real magnetic field, e.g., to the magnetic inclination (dip), is defined as follows:

$$\tan \mu = I / \sqrt{\cos \Phi},$$

where  $\mu$  is the modip latitude,  $I$  is the true magnetic dip (usually at a height of 350 km), and  $\Phi$  is the geographic latitude. Modip equator is the locus of points where the magnetic dip (or inclination) is 0. In the equatorial zone, the lines of constant modip are practically identical to those of the magnetic inclination, but as latitude increases, they deviate and come nearer to those of constant geographical latitude. The poles are identical to the geographic ones [Azpilicueta *et al.*, 2006]. Then, for the purpose of this study, the global TEC data were rearranged in terms of the coordinate system of modip latitude, from  $-80^\circ$  to  $80^\circ$  at each  $5^\circ$ , and geographic longitude, from  $-180^\circ$  to  $180^\circ$  at each  $15^\circ$ . The TEC data falling into the area  $5^\circ$  (modip latitude)  $\times$   $15^\circ$  (longitude) were averaged. The time resolution of 1 h is used in this study, and the hourly data are obtained by interpolation of the 2-hourly original data.

[10] In this study the geomagnetic activity is defined by the global  $K_p$  index; it describes the mean value of the disturbances in the two horizontal geomagnetic field components, observed at 13 selected subauroral stations. The  $K_p$  index data are downloaded from the Space Physics Interactive Data Resource (SPIDR), Boulder, Colorado for the considered period of time. The  $K_p$  value at every hour is used in this study as it is obtained by linear interpolation of the 3 h  $K_p$  values.

[11] In the model, the TEC response to the geomagnetic activity is investigated by the relative deviation of the TEC defined as follows:  $r\text{TEC} = (\text{TEC}_{\text{obs}} - \text{TEC}_{\text{med}}) / \text{TEC}_{\text{med}}$ . The terms  $\text{TEC}_{\text{obs}}$  and  $\text{TEC}_{\text{med}}$  represent observed and median TEC values respectively at a given hour. In the present study we use sliding medians defined by a 15 day moving window, and the median value is assigned to the last day of the window, i.e., to the fifteenth day of the window. We use such type of “one-sided” median approach because in this case the model is built in a way as it will be used for nowcasting or short-term prediction (usually 24 h ahead). In other words, we try to predict the correction to the 15 day median values for each hour of the prediction period. The basic aim of this model is to detect and correctly describe those CODE  $r\text{TEC}$  anomalies which are generated by geomagnetic disturbances. Such anomalies have usually time scales of several days. The 15 day window is used because

of two reasons: (i) the contribution of the  $\sim 27$  day rTEC oscillation due to the solar rotation variability of the EUV radiation is significantly weakened, and (ii) such window has an insignificant effect on the 9 and 13.5 day recurrent geomagnetic activity oscillations which are particularly strong during the declining phase of the solar activity. By considering the characteristic rTEC, the effect of the regular seasonal, diurnal, and solar changes is removed from the TEC variability. The data are grouped into 12 month bins as every bin contains all the available hourly data within the respective month of the year.

### 3. Cross-Correlation Analysis Between rTEC and $K_p$ Index and Its Theoretical Substantiation

[12] The investigations on the  $f_oF_2$  response to the geomagnetic activity, presented by *Muhtarov and Kutiev* [1998] and *Kutiev and Muhtarov* [2003], indicated that this is a delayed response. The authors expressed the delay in terms of the time constant of their cross-correlation function and found a time delay constant of about 18 h. Then the first step in this study is to calculate the 2-D cross-correlation functions between the  $K_p$  index and rTEC.

#### 3.1. Empirical Cross-Correlation Functions

[13] It has been already mentioned that the planetary  $K_p$  index is used in this study as an indicator of the geomagnetic activity. This index reflects both types of variability: from the equatorial ring current and the auroral currents. The effect of geomagnetic activity, described by the  $K_p$  index, on the rTEC variability is investigated by 2-D cross-correlation analysis between both parameters. In the case of building global TEC model, we expect that the cross-correlation function will depend on the season, modip latitude, longitude, and LT. Due to these dependences, three different types of 2-D cross-correlation functions are calculated: (i) longitude-time lag; (ii) LT-time lag, and (iii) modip latitude-time lag. The 2-D cross-correlation functions are calculated for each month of the year because they depend on the season as well. Only some examples of the above mentioned three types of the 2-D cross-correlation functions will be shown here through which the main features of the geomagnetic effects on the rTEC can be demonstrated.

[14] Figure 1 presents 2-D (longitude-time lag) cross-correlation functions calculated between the rTEC and  $K_p$  index for January at different modip latitudes: equator (topmost),  $\pm 20^\circ$  (top row),  $\pm 40^\circ$  (middle row) and  $\pm 70^\circ$  (bottom row). The 2-D cross-correlation functions from both hemispheres are shown in order to demonstrate the seasonal dependence of the TEC response to the geomagnetic activity; winter in the Northern Hemisphere (NH) and summer in the Southern Hemisphere (SH). The time lag up to 72 h is shown because, in general, the response is composed of two phases, positive and negative with different duration and time delay. Some main features of the cross correlation can be distinguished from Figure 1: (i) the rTEC response to the  $K_p$  index shows clear longitude and even some wave-like dependence; in the NH (winter), a wave number 3 response can be seen, while in the SH (summer) and over the equator, in general, wave number 2 can be clarified; (ii) two types of response, positive and negative, can be seen at all plots (the zero time lag is marked by thick black line); first, the response is

positive at all modip latitudes except that at  $70^\circ\text{S}$  (i.e., summer high latitudes where the cross correlation reaches maximum of  $-0.5$  with an average time lag of 6 h), and then it is negative; above the equator, it is mainly positive; (iii) the maximum positive cross correlation of  $+0.4$  is seen at winter high latitudes ( $70^\circ\text{N}$ ), which is reached in the frame of 1–3 h after the maximum  $K_p$  index; by decreasing the modip latitude, the time lag for reaching maximum increases, and, above the equator, it is on the average after  $\sim 9$  h. Some of the longitudinal differences could be caused by the offset of the dipole, an effect that introduces a competition between winds and magnetospheric influence as a function of longitude [*Mendillo et al.*, 1992]. The high dip angles in North America lead to strong magnetospheric electric field effects and weaker wind ones, while in the European sector, where the dip angle is smaller, the winds are more effective than the electric fields. The observed wave-like longitudinal structures could be driven by some nonmigrating tides and stationary planetary waves. The results from Figure 1 reveal that, in the global rTEC model, a dependence on the longitude has to be included.

[15] Figure 2 shows 2-D (LT-time lag) cross-correlation functions calculated between the rTEC and  $K_p$  index for September at the same modip latitudes as in Figure 1. In this case an equinoctial month is shown, autumnal month in the NH and vernal month in the SH. Again, two types, positive and negative, of the rTEC response are seen at all plots. The following cross-correlation features can be summarized from Figure 2: (i) low-latitude rTEC response is mainly positive; the negative response is reached at large time lags; the maximum positive correlations are obtained between 8–10 LT and 18–20 LT with an average time lag of 6–9 h for the tropics and 9–12 h above the equator; (ii) middle-latitude ( $\pm 40^\circ$ ) rTEC response clearly indicates first positive and then negative phases with different durations; the maximum positive coefficients are reached during the daytime 10–12 LT and around midnight with time lags of  $\sim 3$  h for the NH and between 3 and 6 h for the SH; the negative response is stronger for the NH than that in the SH reaching maximum around 2–4 LT and  $\sim 18$  LT; (iii) high-latitude ( $\pm 70^\circ$ ) rTEC response is defined by negative phase during the day (6–20 LT) and a positive, almost instantaneous (zero time lag) response during the night; the negative response in the NH is stronger than that in the SH. The results from Figure 2 reveal that, in the global rTEC model, a dependence on the LT has to be included as well.

[16] Figure 3 presents the 2-D (modip latitude-time lag) cross-correlation functions calculated between the rTEC and  $K_p$  index for different months, January (top row), March (second row), June (third row), and September (bottom row), and at two longitudes,  $0^\circ\text{E}$  (left column) and  $270^\circ\text{E}$  (right column). Again, two types of rTEC response can be seen with different duration and time lag, which depends on the season and modip latitudes. In general, (i) the tropical latitudes at all seasons have positive response with large time lags; (ii) while the winter high-latitude rTEC has first positive response with short time lags and then weak negative one, the summer rTEC demonstrates only negative response; (iii) the middle-latitude (up to  $\pm 50^\circ$ ) rTEC response shows first a weak positive response with short time lags and then stronger negative response with large time lags. Considering all months of the rTEC responses, the following feature can be drawn: the

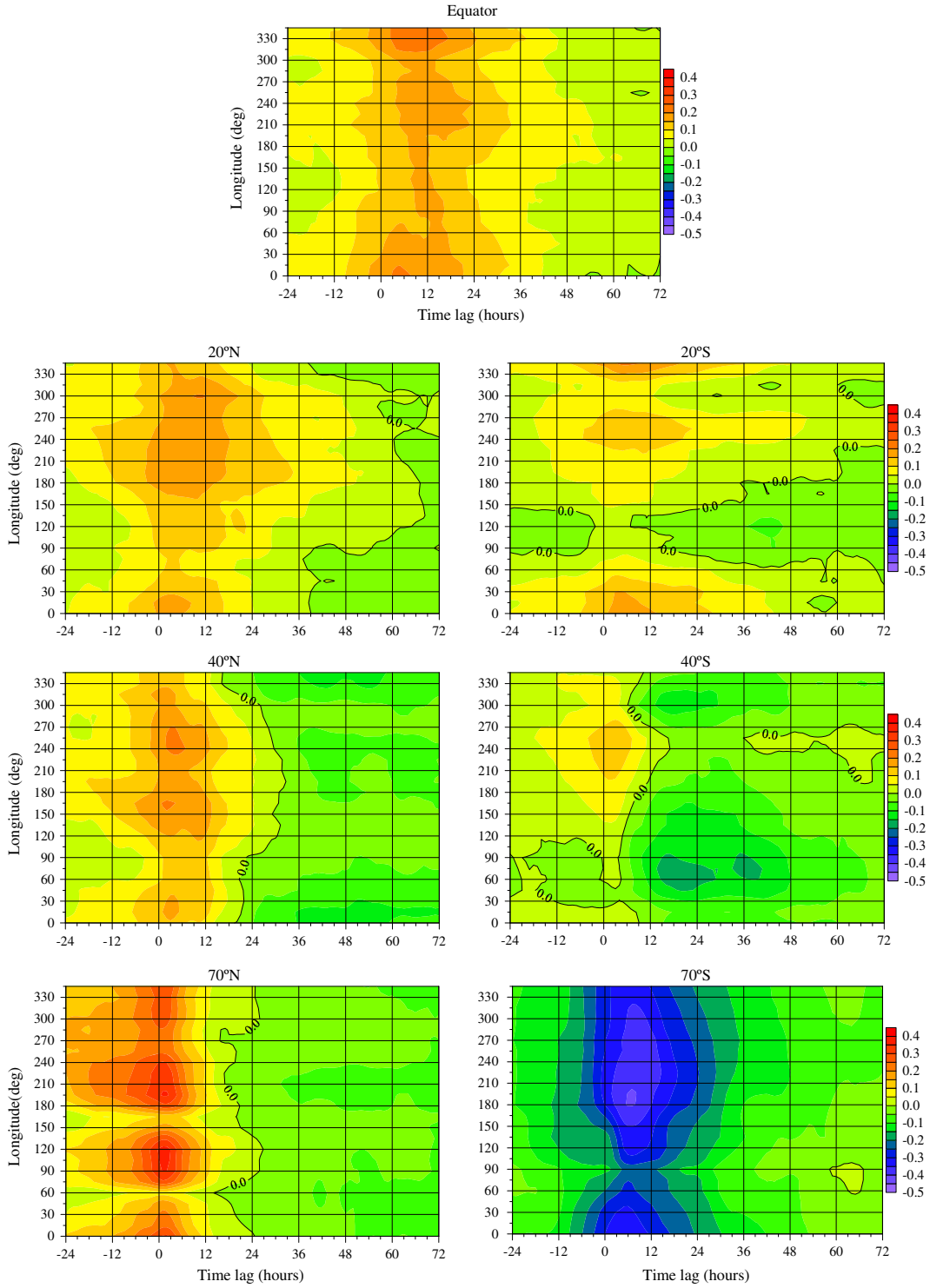


**Figure 1.** Two-dimensional (longitude-time lag) cross-correlation functions calculated between the rTEC and  $K_p$  index for January at (topmost) equator, (top row)  $\pm 20^\circ$ , (middle row)  $\pm 40^\circ$ , and (bottom row)  $\pm 70^\circ$ ; the zero time lag is marked by thick black line.

rTEC response in March/April is close to the winter response in the NH/SH and to the summer one in the SH/NH, while the rTEC response in September/October is close to the summer response in the NH/SH and to the winter response in the SH/NH. Similar result, but only for the NH, was found in the regional TEC model reported by *Andonov et al.* [2011].

### 3.2. Theoretical Cross-Correlation Function Between rTEC and $K_p$ Index

[17] The main conclusion from all types of cross-correlation functions, shown in Figures 1, 2, and 3, is the existence of two types of the rTEC response, positive and negative, with different durations and time lags. Both responses depend on the

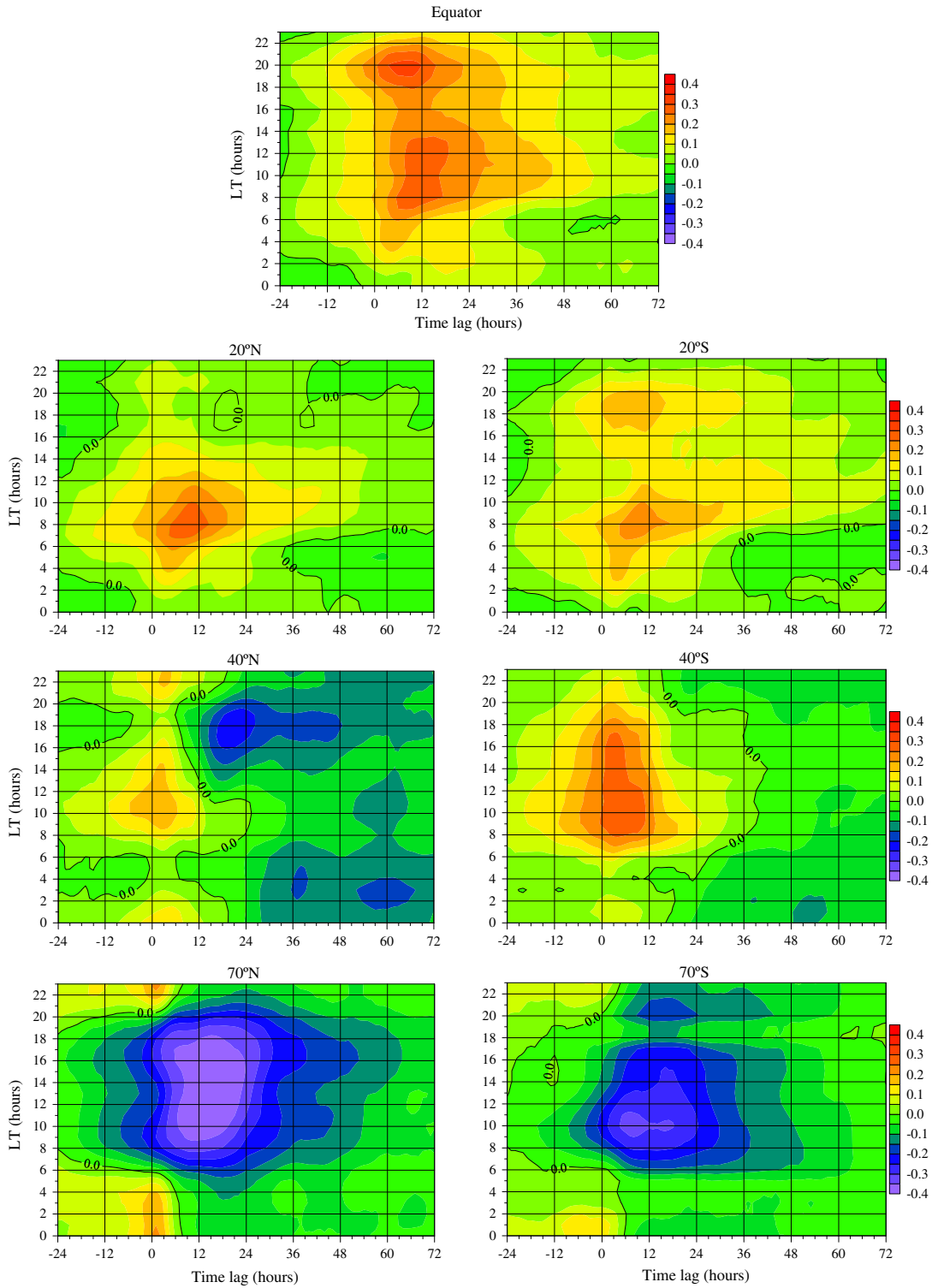


**Figure 2.** Two-dimensional (LT-time lag) cross-correlation functions calculated between the rTEC and  $K_p$  index for September at (topmost) equator, (top row)  $\pm 20^\circ$ , (middle row)  $\pm 40^\circ$ , and (bottom row)  $\pm 70^\circ$ ; the zero time lag is shown by thick black line.

longitude, modip latitude, season, and LT. The cross-correlation results can be used for supporting the use of two different time constants in building the global empirical rTEC model in a way as it has been already done in the regional rTEC model

over American sector [Andonov et al., 2011]. The use of two different time constants hints for the simultaneous action of at least two different processes that define the rTEC response to geomagnetic activity [Mendillo et al., 1992; Mikhailov

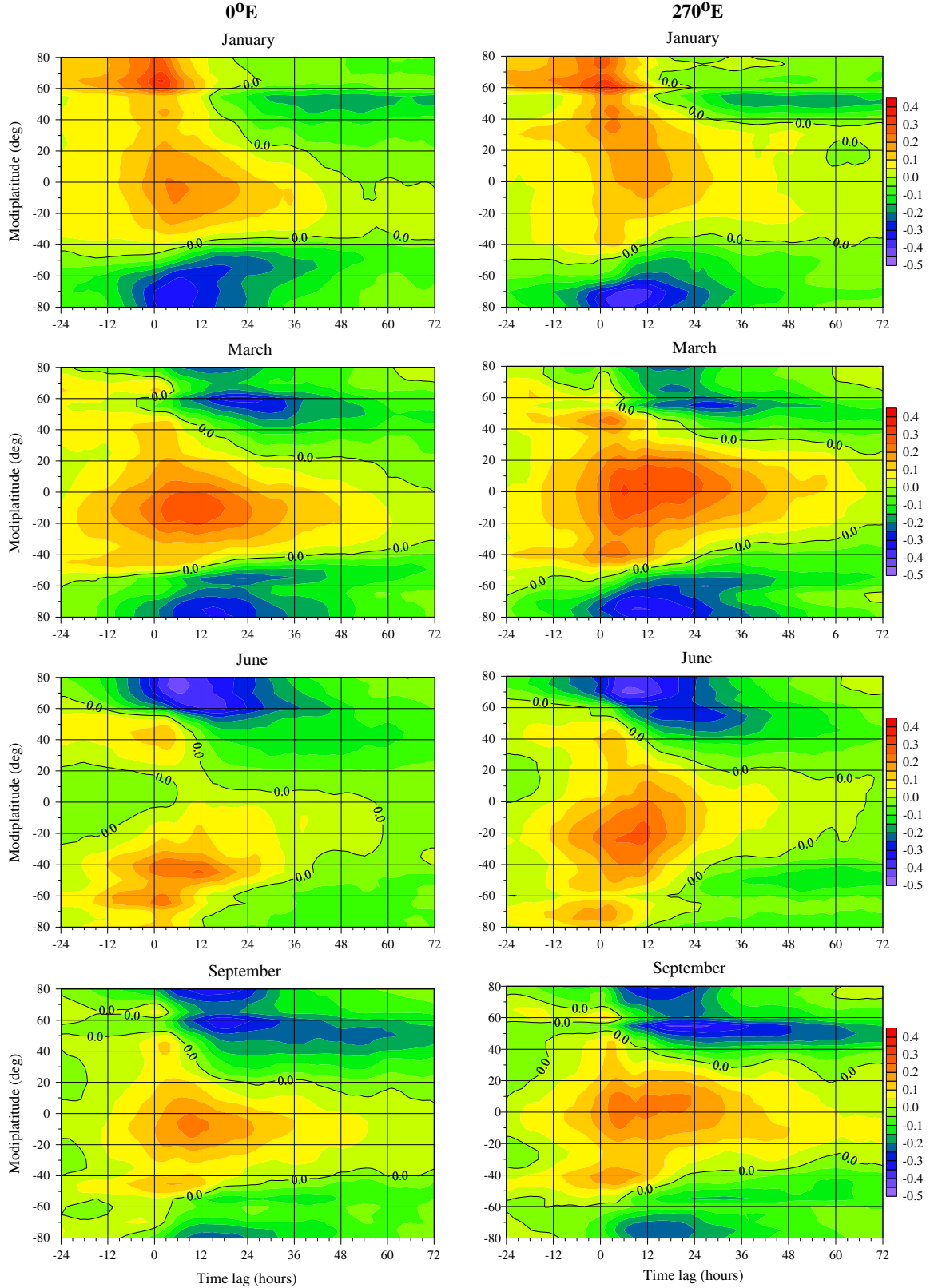


**Figure 3.** Two-dimensional (modip latitude-time lag) cross-correlation functions calculated between the rTEC and  $K_p$  index for months: (top row) January, (second row) March, (third row) June, and (bottom row) September and at (left column) 0°E and (right column) 270°E; the zero time lag is shown by thick black line.

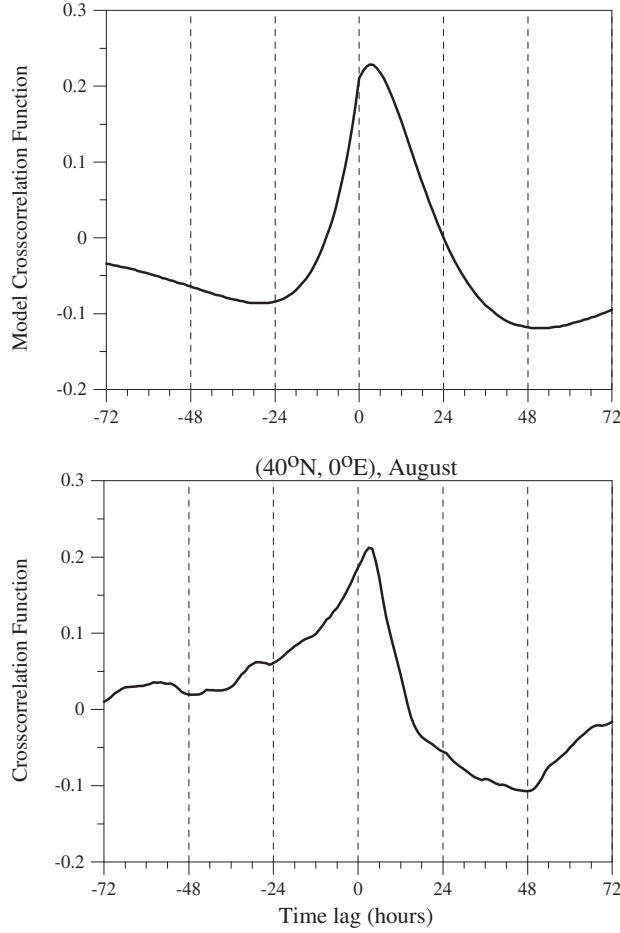


**Figure 4.** Comparison between the (top) theoretical cross-correlation function calculated for  $T_1 = 12$  h,  $T_2 = 32$  h,  $\alpha = 1$ ,  $\beta = -1$  and for simplicity the variance is accepted to be 1, and (bottom) the empirical cross-correlation function between the  $K_p$  index and rTEC for August and at  $(40^\circ\text{N}, 0^\circ\text{E})$ .

and Schlegel, 1998; Prölss, 2005]. The existence of at least two processes is considered also in Mukhtarov and Pancheva [2012] where the ionospheric response to the high-speed solar wind streams is studied by using the COSMIC electron density measurements.

[18] A method for modeling the cross-correlation function between the relative  $f_oF_2$  and the geomagnetic index is described in Muhtarov *et al.* [2002], where the delayed response

is represented by a linear filter from the first order. A similar approach was applied in this study in order to theoretically base the use of two different time constants in establishing the global rTEC model response to the geomagnetic activity.

[19] If we assume that the temporal variability of the geomagnetic index can be described as a stationary random process (for simplicity noted as  $x(t)$ ) while the rTEC (noted here as  $y(t)$ ) is a result of converting the geomagnetic activity by two independent linear filters from the first order, then

$$y(t) = \alpha \int_{-\infty}^{\infty} h_1(\xi)x(t - \xi)d\xi + \beta \int_{-\infty}^{\infty} h_2(\xi)x(t - \xi)d\xi \quad (1)$$

[20] The transition functions of both filters can be denoted as follows:

$$h_1(t) = \begin{cases} \frac{1}{T_1} \exp\left(-\frac{t}{T_1}\right), & t \geq 0 \\ 0, & t < 0 \end{cases}$$

$$h_2(t) = \begin{cases} \frac{1}{T_2} \exp\left(-\frac{t}{T_2}\right), & t \geq 0 \\ 0, & t < 0 \end{cases} \quad (2)$$

[21] Thus, the ionospheric response is represented as a linear combination of two delayed responses with time delay constants respectively  $T_1$  and  $T_2$  and coefficients of proportionality respectively  $\alpha$  and  $\beta$ . Actually, the ionospheric response is not a deterministic process; hence, the above mentioned quantities have to be interpreted as characteristics of the most probable response at given conditions.

[22] The cross-correlation function between the processes  $x$  and  $y$  is described by the interrelations of Wiener-Lee:

$$R_{xy}(\tau) = \int_{-\infty}^{\infty} (\alpha h_1(\xi) + \beta h_2(\xi))R_{xx}(\tau - \xi)d\xi \quad (3)$$

[23] The autocorrelation function of the geomagnetic activity can be represented with sufficient accuracy [Muhtarov *et al.*, 2002] by an exponential function:

$$R_{xx}(\tau) = \sigma_x^2 \exp\left(-\frac{|\tau|}{T_g}\right) \quad (4)$$

where the magnitude of the logarithmic decrement of  $R_{xx}(\tau)$  is approximately 14 h [Muhtarov *et al.*, 2002]. Having in mind the above mentioned assumptions, then the cross-correlation function can be expressed as follows:

$$R_{xy}(\tau) = \sigma_x^2 \left[ \alpha \left( \frac{T_g}{(T_1 - T_g)} \left( \frac{2T_1}{(T_1 + T_g)} \exp\left(-\frac{\tau}{T_1}\right) - \exp\left(-\frac{\tau}{T_g}\right) \right) \right) + \beta \left( \frac{T_g}{(T_2 - T_g)} \left( \frac{2T_2}{(T_2 + T_g)} \exp\left(-\frac{\tau}{T_2}\right) - \exp\left(-\frac{\tau}{T_g}\right) \right) \right) \right] \quad \tau \geq 0$$

$$R_{xy}(\tau) = \sigma_x^2 \left[ \alpha \left( \frac{T_g}{(T_1 + T_g)} \exp\left(\frac{\tau}{T_1}\right) \right) + \beta \left( \frac{T_g}{(T_2 + T_g)} \exp\left(\frac{\tau}{T_2}\right) \right) \right] \quad \tau \leq 0 \quad (5)$$

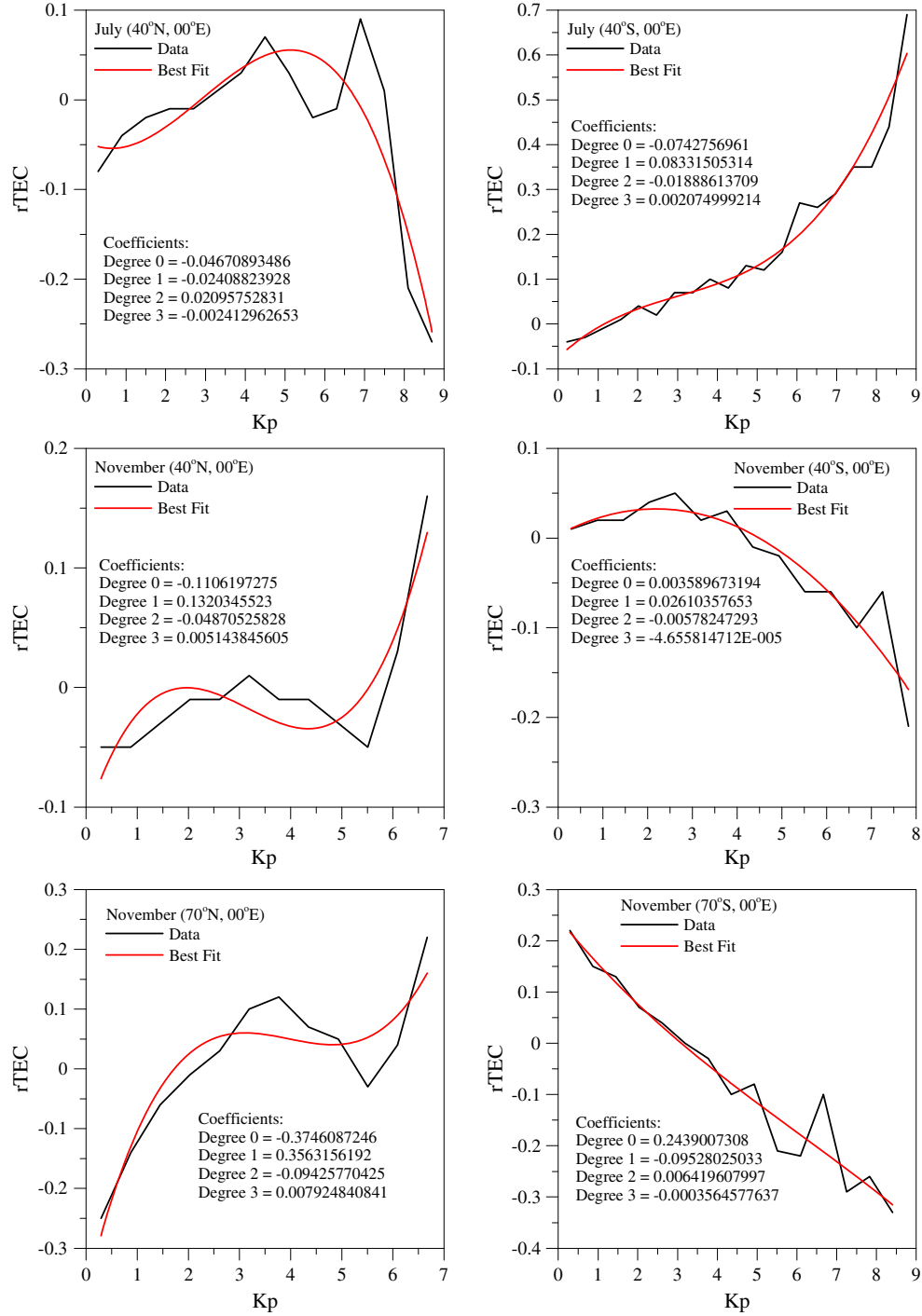


**Figure 5.** The empirical dependence between the  $K_p$  and  $rTEC$  calculated for different months and geographical points noted at the plots.

[24] At  $\tau=0$ , both expressions and their first derivatives become equal. Figure 4 shows a comparison between the theoretical (described by formula (5)) cross-correlation function calculated for  $T_1 = 12$  h,  $T_2 = 32$  h,  $\alpha = 1$ , and  $\beta = -1$ , and for simplicity the variance of the geomagnetic activity is accepted to be 1 (Figure 4, top) and the empirical cross-correlation function between the  $K_p$  index and  $rTEC$  for August and at (40°N, 0°E) (Figure 4, bottom). It is seen that the main features of the two cross-correlation functions are very similar: a positive response with small time lag followed

by a negative response with longer time lag. The assumption that the sum response is shaped by two responses, a positive with small time constant and a negative one with three times longer time constant, is set in the model. In this way, at the range of positive time lag, a near area of positive correlation and a distant area of negative correlation are formed. In the presence of only one process, it is impossible for both positive and negative correlations to be obtained. The investigation of the relative  $f_oF_2$  response to the geomagnetic activity in summer at the middle latitudes reported by *Muhtarov et al.*

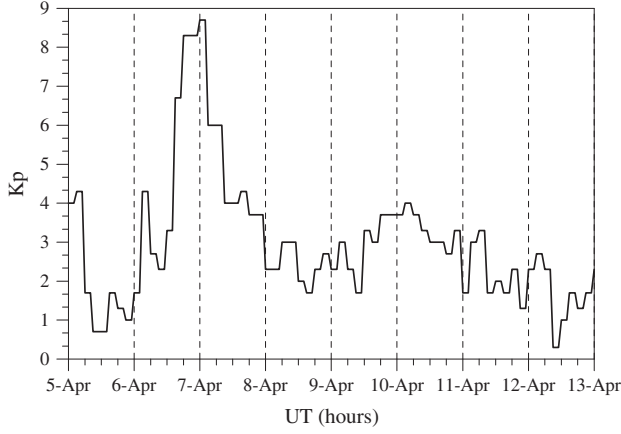


**Figure 6.** (a) Temporal variability of the  $K_p$  index during the geomagnetic storm on 5–13 April 2000. (b) Comparison between observed (left column), the model (middle column), and the difference between them (right column; the zero line is marked by thick white line) TEC longitude-hour cross-sections for the geomagnetic storm on 5–13 April 2000 at different modip latitudes noted above the plots. (c) Temporal variability of the systematic error (in TECU, blue color) and the RMSE (in TECU, red color) presented for each day of the geomagnetic storm on 5–13 April 2000.

[2002] and *Kutiev and Muhtarov* [2003] indicated that the response is negative. In this study, however, the rTEC response at the same conditions is composed of positive and negative responses. This means that the positive response of the rTEC should be due to the positive response of the electron density above the  $F$  region maximum. *Mukhtarov and Pancheva* [2012, Figure 5], shows the altitude distribution of the amplitudes and phases of the COSMIC electron density variability driven by the 9 day recurrent geomagnetic activity. At  $50^\circ\text{N}$  and during the summer (near days 270) two areas of response can be distinguished; one is around 200 km height, and the second is above 300 km height. The phase difference between the oscillations in the electron density and those of the geomagnetic activity for the lower area of response is close to out of phase, i.e. the response is negative, while the phase difference for the upper area of response is close to in phase, i.e., positive response. In the present study, the cross-correlation analysis supports this result; additionally, it reveals also that the two responses have different time delay. We suggested in *Mukhtarov and Pancheva* [2012] that the negative response is due mainly to the changes in neutral composition, i.e., decrease of the  $\text{O}/\text{N}_2$  ratio because of the upwelling and equatorward winds [*Crowley et al.*, 2008], while the positive response is due predominantly to the  $F_2$  peak that has moved upward during a storm [*Pröls, 1995; Buonsanto, 1999; Mendillo, 2006*] and to an enhancement in the electron density scale height because the ion temperature in the  $F$  region shows enhancements [*Sojka et al.*, 2009]. The negative response practically disappears over the equator, and it is mainly due to the increase of the  $\text{O}/\text{N}_2$  ratio changes because of downwelling winds [*Pröls, 1995; Crowley et al.*, 2008].

#### 4. Basic Approach of the Model Construction

[25] The basic idea of each global empirical TEC model which describes the response to the geomagnetic activity is

to define a set of analytical expressions which describe the most probable TEC values at given geomagnetic activity index, day of the year, geographic location, and LT. The investigations on the  $f_oF_2$  response to the geomagnetic activity [*Muhtarov et al.*, 2002; *Wang et al.*, 2008] indicated that this is a delayed response which can be satisfactorily modeled by assuming that the geomagnetic influence is imposed on the inertial system described by an inhomogeneous differential equation from a first order [*Kutiev and Muhtarov, 2003*]. In the present study, the cross-correlation analysis, however, indicated that the rTEC response to the geomagnetic activity has to be presented by a sum of two responses with different time delay constants and with different signs of the cross-correlation function. It is known also that during the recovery phase of the ionospheric storms with geomagnetic origin, the ionospheric reaction continues some time after the geomagnetic storm attenuation. This phenomenon aggravates the relationship between the  $K_p$  index and the ionospheric anomalies. In order to resolve this problem, *Muhtarov et al.* [2002] suggested an approach for defining new modified function of  $K_p$  index based on the time delay constant from the cross-correlation analysis, with its variations closely resembling those of the relative  $f_oF_2$ . Having in mind the above mentioned ideas, *Andonov et al.* [2011] constructed regional rTEC model over North America and a similar approach will be used in the present study as well.

[26] If we assume that the impact of the geomagnetic activity on the rTEC is accomplished by two mechanisms with different time delay constants, then the variability of rTEC can be described as follows:

$$\text{rTEC}(t) \approx (f_{T_s}(Kp_{T_s}(t)) + f_{T_l}(Kp_{T_l}(t)))f_{lt}(\text{LT})f_{lon}(\text{Lon}) \quad (6)$$

where the functions  $f_{lt}(\text{LT})$  and  $f_{lon}(\text{Lon})$  represent the dependence of the rTEC response on the LT and longitude at equal other conditions.  $Kp_{T_s}$  and  $Kp_{T_l}$  are the modified parameters with the time delay constants respectively  $T_s$  and  $T_l$  values of the  $K_p$  index. These modified parameters are solutions of the equations shown below and are obtained easily by a numerical integration:

$$T_s \frac{dKp_{T_s}(t)}{dt} + Kp_{T_s}(t) = Kp(t) \quad (7)$$

$$T_l \frac{dKp_{T_l}(t)}{dt} + Kp_{T_l}(t) = Kp(t) \quad (8)$$

[27] The unknown functions  $f_{T_s}$  and  $f_{T_l}$  from (1) can be expressed by the Taylor series expansions while the dependence on the LT and longitude can be presented by Fourier series as follows:

$$\begin{aligned} f_{T_s}(Kp_{T_s}) &= \alpha_{0s} + \alpha_{1s}Kp_{T_s}(t) + \alpha_{2s}Kp_{T_s}(t)^2 + \alpha_{3s}Kp_{T_s}(t)^3 + \dots \\ f_{T_l}(Kp_{T_l}) &= \alpha_{0l} + \alpha_{1l}Kp_{T_l}(t) + \alpha_{2l}Kp_{T_l}(t)^2 + \alpha_{3l}Kp_{T_l}(t)^3 \dots \\ f_{lt}(\text{LT}) &= \beta_0 + \sum_{i=1}^4 \beta_i \cos\left(i \frac{2\pi}{24} \text{LT} - \phi_i\right) \\ f_{lon}(\text{Lon}) &= \gamma_0 + \sum_{i=1}^6 \gamma_i \cos\left(i \frac{2\pi}{24} \text{Lon} - \psi_i\right) \end{aligned} \quad (9)$$

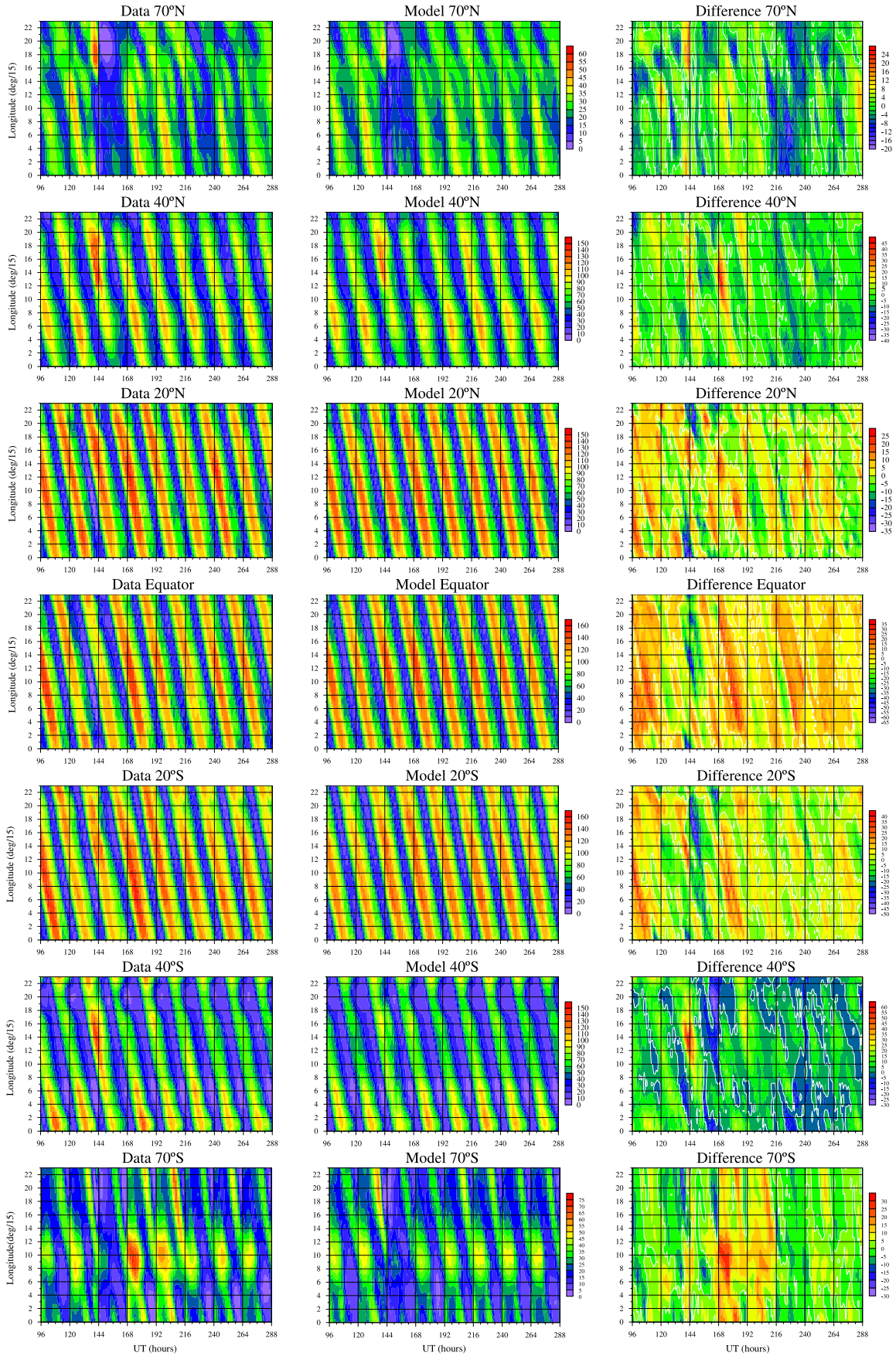
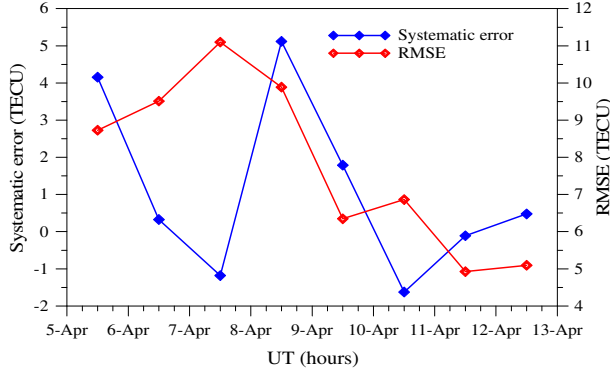


Figure 6. (continued)



**Figure 6.** (continued)

[28] Then the rTEC can be described as follows:

$$\text{rTEC}(Kp_{T_s}, Kp_{T_l}, \text{LT}, \text{Lon}) = \left( \begin{array}{l} (\alpha_{0s} + \alpha_{1s}Kp_{T_s}(t) + \alpha_{2s}Kp_{T_s}(t)^2 + \alpha_{3s}Kp_{T_s}(t)^3) + \\ (\alpha_{0l} + \alpha_{1l}Kp_{T_l}(t) + \alpha_{2l}Kp_{T_l}(t)^2 + \alpha_{3l}Kp_{T_l}(t)^3) \end{array} \right) \times \quad (10)$$

$$\left( \beta_0 + \sum_{i=1}^4 \beta_i \cos\left(i \frac{2\pi}{24} \text{LT} - \phi_i\right) \right) \times \left( \gamma_0 + \sum_{i=1}^6 \gamma_i \cos\left(i \frac{2\pi}{24} \text{Lon} - \psi_i\right) \right)$$

[29] We note that the Fourier time series (third relation in (9)) includes the contribution of four harmonics, 24, 12, 8, and 6 h, while the Fourier longitude series (fourth relation in (9)) includes the contribution of six harmonics, i.e., the contribution of zonal waves with zonal wave numbers up to 6. It is worth noting that the numbers of the included components in the Fourier expansion series are defined experimentally. We accepted only the contribution of the above mentioned diurnal components and zonal waves because the addition of more components does not decrease the model error. The following criterion was used: the addition of more components has been discarded when their inclusion leads to an error improvement only after the third decimal point.

[30] The next important step is to find a functional dependence between the  $K_p$  and rTEC in order to clarify the number of terms in the Taylor series (first two relations in (9)). The most appropriate type of the functional dependence is defined empirically by an approach described in *Andonov et al.* [2011]. Some examples of the empirical dependence between the  $K_p$  and rTEC calculated for different months and geographical points, which are denoted at the plots, are presented in Figure 5. It is evident that in all cases the functional dependence between  $K_p$  and rTEC is close to the cubic function. Due to this result in the Taylor series, only the contributions of the first four terms are included. Then the most probable values of the coefficients:  $\alpha_{is}$ ,  $\alpha_{il}$ ,  $\beta_i$ ,  $\gamma_i$ ,  $T_s$ , and  $T_l$  from 9 have to be determined. This is a nonlinear optimizing task that can be solved by applying the “trial-and-error” method in a way that the best approximation in a sense of minimum least squares deviation is to be assured. In order to solve the problem, the following steps are made: (i) it is given a range of  $T_s$  changes from 0 to 10 h with a time

resolution of 1 h and a range of  $T_l$  changes from 11 to 72 h with a time resolution also of 1 h; (ii) for each point of the grid built in this way the coefficients  $\alpha_{is}$ ,  $\alpha_{il}$ ,  $\beta_i$ , and  $\gamma_i$  are found by using the method of least squares best fit, and (iii) the coefficients  $\alpha_{is}$ ,  $\alpha_{il}$ ,  $\beta_i$ ,  $\gamma_i$ ,  $T_s$ , and  $T_l$  at which the best approximation (in a sense of minimum least squares deviation) is obtained are accepted as optimal coefficients for the model rTEC described by (10).

[31] In the present study we accepted the following: (i) longitude and UT as independent variable quantities; the conversion to LT is a simple procedure and (ii) at each modip latitude, a separate model, described by 10, is constructed; the values of the model rTEC which do not belong to the  $5^\circ$  modip grid are obtained by an interpolation procedure that will be described later. The latter is done because if a latitudinal approximation is used first, the number of model constants will increase and, second, an

additional error will be introduced. The rTEC model described by (10) contains 820 constants, and they are determined by least squares fitting techniques.

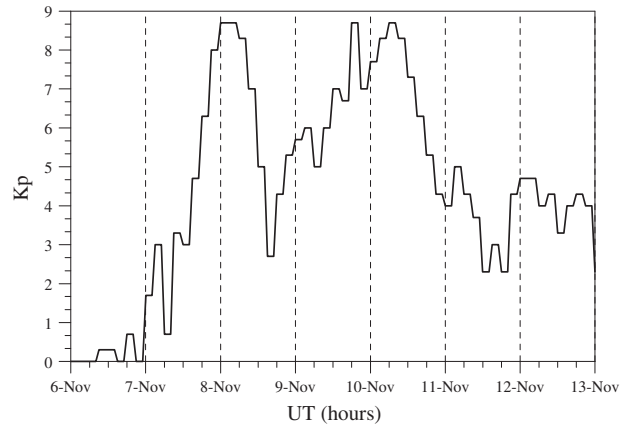


**Figure 7.** (a) Temporal variability of the  $K_p$  index during the geomagnetic storm on 6–13 November 2004. (b) Comparison between observed (left column), the model (middle column), and the difference between them (right column; the zero line is marked by thick white line) TEC longitude-hour cross-sections for the geomagnetic storm on 6–13 November 2004 at different modip latitudes noted above the plots. (c) Temporal variability of the systematic error (in TECU, blue color) and the RMSE (in TECU, red color) presented for each day of the geomagnetic storm on 6–13 November 2004.

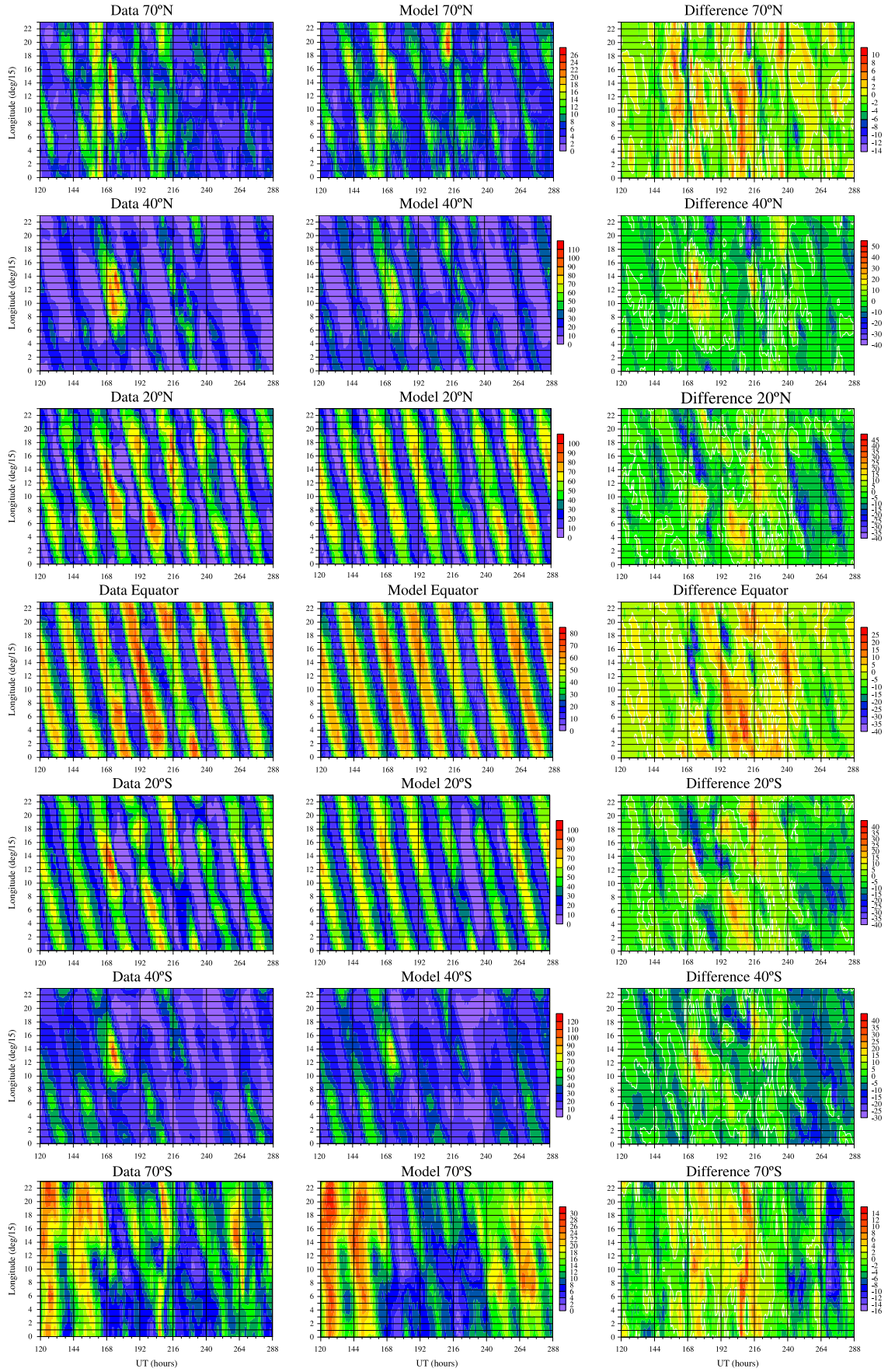


Figure 7. (continued)

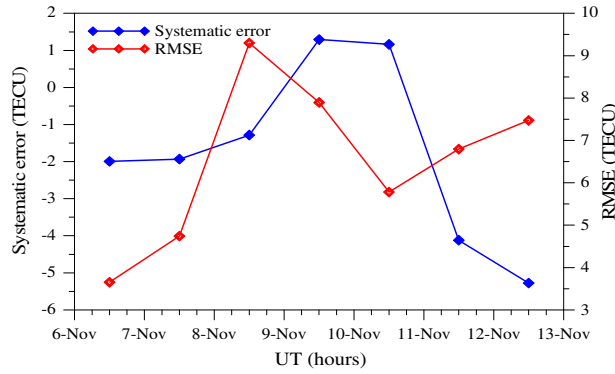


Figure 7. (continued)

## 5. Model Results

[32] In order to demonstrate how the model is able to describe the rTEC response to geomagnetic activity, three geomagnetic storms observed at different seasons and solar activity conditions will be presented. The results, however, will be presented as a corrected 15 day median TEC with the model rTEC, where  $TEC_{mod} = TEC_{med}(1 + rTEC)$ .

[33] Figure 6a shows the temporal variability of the  $K_p$  index during the geomagnetic storm on 5–13 April 2000, i.e., at high solar activity. The rapid increase of the  $K_p$  index starts at around 12 UT on 6 April and reaches the largest values (close to 9) at midnight and early hours on 7 April; then it decreases to the undisturbed levels. Figure 6b presents the comparison between the CODE data (left column), model result (middle column), and the difference of the (right column) TEC longitude-hour cross sections for the considered period of time, 5–13 April 2000 at different modip latitudes which are noted above the plots. We clarify that the longitude is presented by numbers defined from longitude/15°, while the time is in hours, and it starts on 1 April 2000 at 00 UT. In order to facilitate the comparison between the CODE data and model results, the color scales (in TECU) are the same at the same modip latitudes. However, as the TEC response strongly depends on the modip latitude, the color scales are different at different modip latitudes. The careful comparison between model and data plots reveals that the model overall well reproduces the real situation. It, however, underestimates with ~12–14 TECU at longitudes of 240–300° the positive TEC response at 70°N in the second half of 6 April, i.e., almost simultaneously with the largest values of  $K_p$  index, and 1 day later, positive response at 70°S with ~25–30 TECU at longitudes of 90–180°. The model quite well reproduces the negative TEC response in the second half of 6 April at 70°S when  $K_p$  index rapidly increases, as well as the response on the next day (the difference is close to zero). At middle latitudes,  $\pm 40^\circ$ , the model positive TEC response is also slightly underestimated in the second half of 6 April; the difference between the CODE data and the model is smaller at 40°N (~10–15 TECU) than at 40°S (~50–55 TECU at around longitude of 200°). The model TEC response at tropical and equatorial latitudes comparatively well reproduces the data, but again, it underestimates the positive response above the equator seen on 8 April (the difference reaches ~30 TECU). It is worth noting that, at all modip latitudes, the model very well describes the longitude variabilities

of the TEC response. Most probably, this is due to the large number of the zonal waves included in the model.

[34] In order to assess how the model reproduces the CODE TEC response to the geomagnetic storm on 5–13 April 2000, we calculate the systematic (mean) error and root mean squares error (RMSE) for each day of the considered geomagnetic storm. They are defined by the first two expressions of (4) from Mukhtarov *et al.* [2013a], and the result is shown in Figure 6c. It is seen that while at the first day of the geomagnetic storm, 6 April, the systematic error (blue color) is almost zero and RMSE (red color) is ~9.5 TECU at the second day, 7 April, the systematic error is ~-1.3 TECU, but the RMSE reaches its maximum of ~11 TECU. The systematic error reaches its maximum of ~5 TECU on 8 April. Figure 6c reveals large positive bias (up to 5 TECU) and RMSE (up to 11 TECU); however, it is worth reminding that the considered geomagnetic storm is at high solar activity.

[35] Figure 7a presents the temporal variability of the  $K_p$  index during the geomagnetic storm on 6–13 November 2004, i.e., during the declining phase of the solar cycle. This is a more complex geomagnetic storm with two  $K_p$  index amplifications which are far from each other of about 2 days. Figure 7b presents the comparison between the TEC longitude-hour cross sections obtained by the CODE data (left column), the model result (middle column), and the difference between them (left column), for the period of time 6–13 November 2004 at different modip latitudes arranged in the same way as those in Figure 6b. In this case the TEC responses to both  $K_p$  index amplifications have to be considered. The model comparatively well reproduces the TEC response related to the first  $K_p$  index amplification at high latitudes,  $\pm 70^\circ$ , but underestimates that connected with the second  $K_p$  index amplification with ~8–12 TECU. The temporal and longitudinal variability of the rTEC response at middle latitudes,  $\pm 40^\circ$ , is well reproduced; however, the positive TEC response

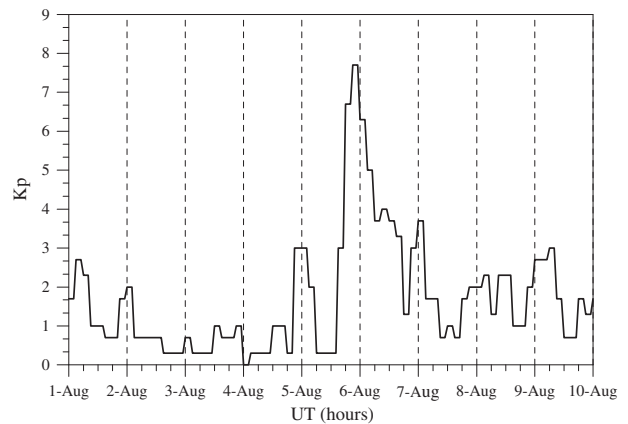


Figure 8. (a) Temporal variability of the  $K_p$  index during the geomagnetic storm on 1–10 August 2011. (b) Comparison between observed (left column), the model (middle column), and the difference between them (right column; the zero line is marked by thick white line) TEC longitude-hour cross sections for the geomagnetic storm on 1–10 August 2011 at different modip latitudes noted above the plots. (c) Temporal variability of the systematic error (in TECU, blue color) and the RMSE (in TECU, red color) presented for each day of the geomagnetic storm on 1–10 August 2011.

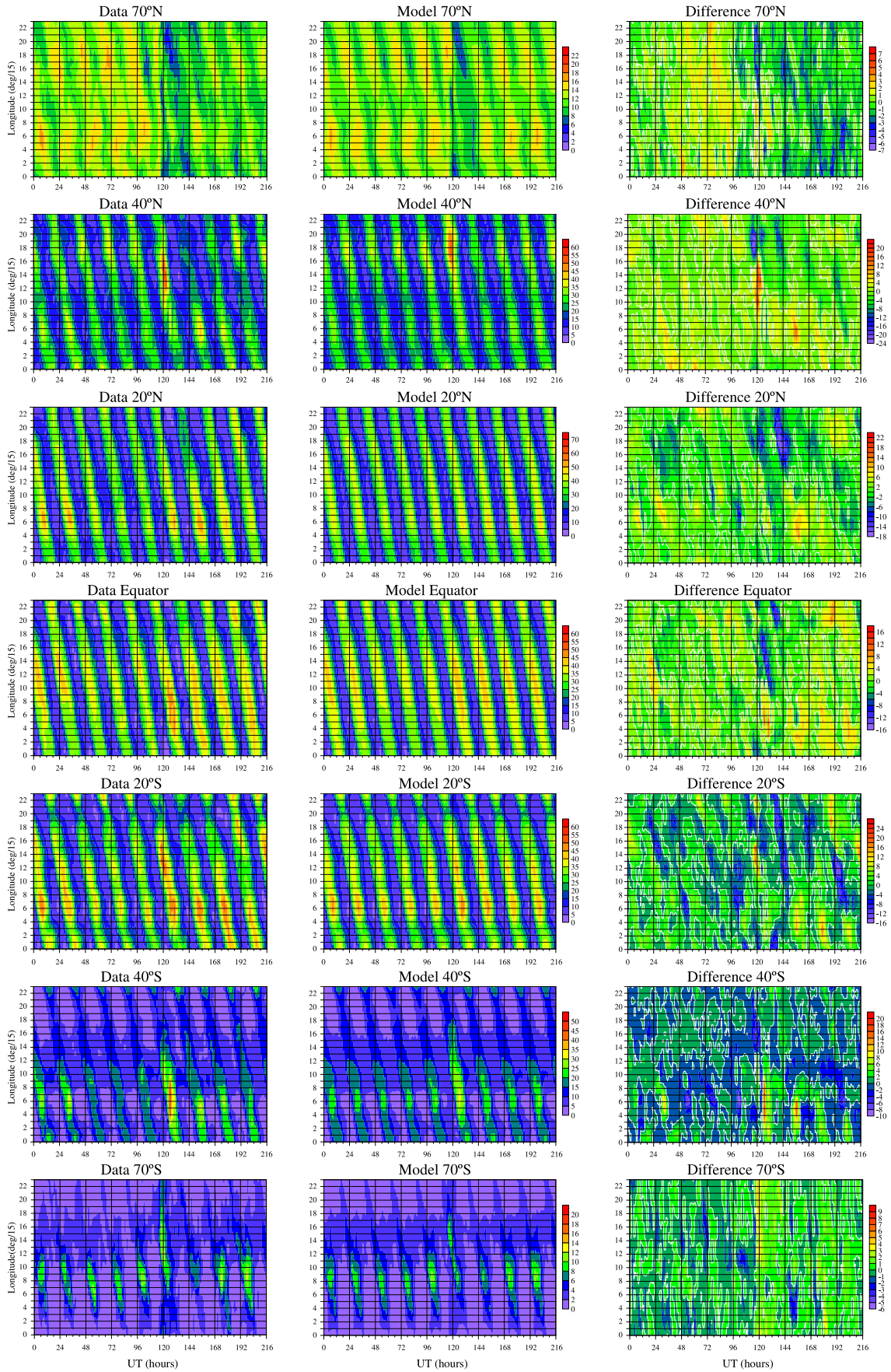
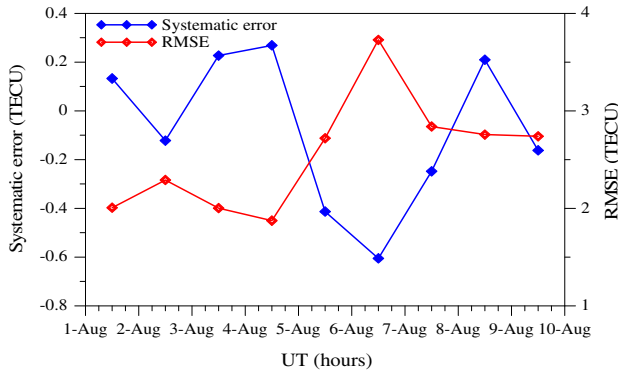


Figure 8. (continued)



**Figure 8.** (continued)

on 8 November is again underestimated by  $\sim 30\text{--}40$  TEC at longitudes of  $\sim 150\text{--}220^\circ$ . Some overestimation of the TEC response on 8 November can be distinguished at some longitudes at tropical and equatorial latitudes, as well as some underestimation of the TEC response on 9 November particularly over the equator. Figure 7c presents the temporal variability of the systematic error (in TECU, blue color) and the RMSE (in TECU, red color) presented for each day of the geomagnetic storm on 6–13 November 2004. It shows that while the systematic error is negative (up to  $-2$  TECU) during the first  $K_p$  index amplification, 7–8 November, it is positive (up to 1 TECU) during the second  $K_p$  index amplification, 9–10 November. The RMSE reaches a maximum of  $\sim 9$  TECU on 8 November and decreases to  $\sim 6$  on 10 November.

[36] Figure 8a presents the temporal variability of the  $K_p$  index during the geomagnetic storm in 1–10 August 2011, i.e., during the increasing phase of the solar cycle. This geomagnetic storm causes negative TEC response at  $70^\circ\text{N}$  and positive one at  $70^\circ\text{S}$ . The model reproduces quite well the temporal and longitudinal TEC variability at high latitudes with slightly weaker magnitude of the response. As it is expected in advance, the TEC response at middle latitudes,  $\pm 40^\circ$ , is characterized by positive response with short time delay and a weak negative response with long time delay. The model reproduces overall well the midlatitude TEC response, but the negative reaction seen in the second half of 6 August and on 7 August, particularly at  $40^\circ\text{N}$ , is underestimated by the model. Additionally, the model positive rTEC response at  $40^\circ\text{N}$  maximizes  $30^\circ$  eastward of that shown by the data. The longitude and temporal variability of the rTEC response at tropical latitudes,  $\pm 20^\circ$ , is well reproduced; only the magnitude of the positive response is slightly weaker than the observations. The rTEC response over the equator as it is expected is positive, and it is well seen in the model results; only the longitude disturbances located between  $45^\circ$  and  $150^\circ$  is not well outlined. Figure 8c shows the temporal variability of the systematic error (in TECU, blue color) and the RMSE (in TECU, red color) presented for each day of the geomagnetic storm on 1–10 August 2011. It is seen that during the disturbed days, 5–7 August, the systematic errors change from  $\sim 0.3$  TEC to  $-0.6$  TECU, while the RMSE changes from  $\sim 2$  TECU to  $\sim 3.7$  TECU.

[37] The above shown examples of three geomagnetic storms clearly indicate that the global empirical TEC model

presented in this paper describes well the ionospheric response to the geomagnetic activity at different solar cycle and seasonal conditions. The differences between the CODE data and the model results at different modip latitudes (the right columns in Figures 6b, 7b, and 8b) clearly demonstrate two types of the model deviation from the data: some underestimation of the largest TEC response to the geomagnetic activity and randomly distributed errors which are actually the data noise or anomalies generated by other sources. The latter is a consequence of the cross-correlation results shown in Figures 1, 2, and 3; the maximum values of the cross-correlations coefficients there reach values of only 0.4–0.5. The presented systematic errors and RMSE for each day of the geomagnetic storms, Figures 6c, 7c, and 8c, reveal the largest values during the disturbed days and at high solar activity.

[38] Each empirical model needs to assess the quality of the adjustment procedure by model residuals, i.e., by calculating the differences between input data and model values. The main statistics based on the entire data set will be presented here. It is worth noting that, actually, the residuals reveal the nature of the modeling error. Due to this, it has been accepted that besides the systematic (mean) error (ME) and RMSE, also the standard deviation error (STDE) is usually accepted as the basic error characteristic of each model. They are defined by the expressions (4) from Mukhtarov *et al.* [2013a]. The following error values for the period of time 1 January 1999 to 31 December 2011 are obtained: ME =  $-0.204$  TECU, i.e., the model fits to the CODE TEC data with small negative bias; then the RMSE and STDE have very close values, i.e., RMSE = 4.592 TECU and STDE = 4.588 TECU.

[39] The overall statistics of the model error can be defined more precisely by showing the dependence of RMSE on modip latitude and months. Figure 9 shows a modip latitude-month cross section of the model RMSE calculated for the entire (January 1999 to December 2011) period of time. The largest RMSE, reaching 7.5 TECU, is observed at low latitudes where the equatorial ionospheric anomaly is developed; the crests are situated at around  $\pm 30^\circ$  modip latitude [Mukhtarov and Pancheva, 2011]. Some amplification of the RMSE can be noticed also around  $70^\circ\text{S}$  during the equinoxes; it reaches around 4 TECU. The largest errors are found mainly in the equinoxes, and this could be due to

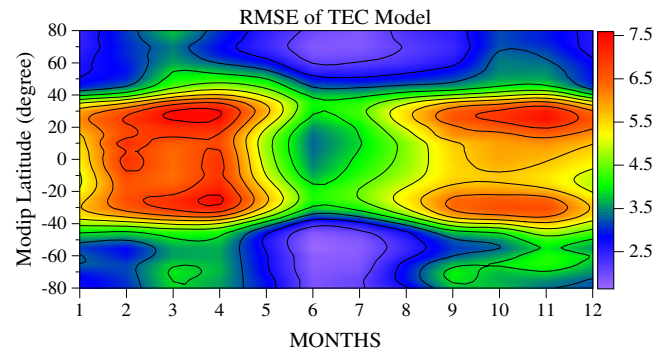


**Figure 9.** Modip latitude-month cross section of the model RMSE calculated for the entire (January 1999 to December 2011) time interval.

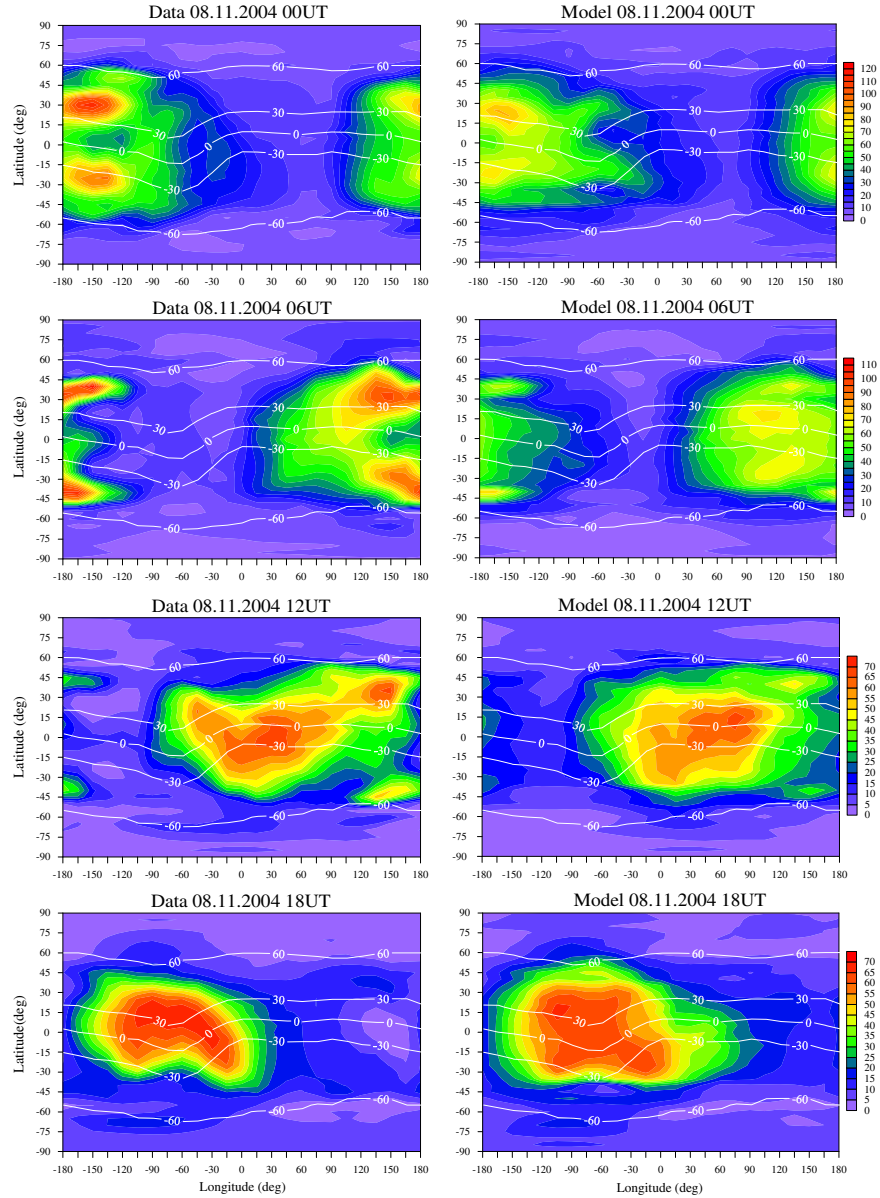


**Figure 10.** Comparison between the (right column) model and CODE TEC maps for 8 November 2004 geomagnetic storm at (top row) 00 UT, (second row) 06 UT, (third row) 12 UT, and (bottom row) 18 UT. The modip latitude is also marked by white line.

both semiannual variability of the ionosphere and semiannual variability of the geomagnetic activity. We calculated also the RMSE for each month of the entire time interval (not shown result); as it is expected in advance that the RMSE has larger values during high solar activity.

## 6. Global TEC Maps

[40] The basic aim of each global TEC model used for short-term prediction is to construct the global distribution of the TEC, i.e., to obtain global TEC maps at given geomagnetic activity, day of the year, and UT. The rTEC model presented in this study predicts the correction to the 15 day median values for each hour of the prediction period. As it has been already mentioned, the TEC value at a given hour is actually a corrected 15 day median TEC with the model

rTEC. Then the TEC maps are constructed by interpolation of the TEC values from the used grid with a  $5^\circ$  step in modip latitude and  $15^\circ$  in longitude. The interpolation between obtained TEC values is done by using Inverse Distance Method [Shepard, 1968]. Then the modip frame is converted to geographical one. The TEC values assigned to both poles are found by interpolation between the known from the model points which have the highest northern and southern latitudes. The model maps are arrayed in terms of the coordinate system of geographical latitude from  $-90^\circ$  to  $90^\circ$  at each  $5^\circ$  and longitude from  $-180^\circ$  to  $180^\circ$  at each  $5^\circ$ .

[41] Figure 10 presents a comparison between the model (right column) and CODE TEC maps for 8 November 2004 geomagnetic storm at 00 UT (top row), 06 UT (second row), 12 UT (third row), and 18 UT (bottom row). In order to facilitate the comparison, the color scales at each pair of

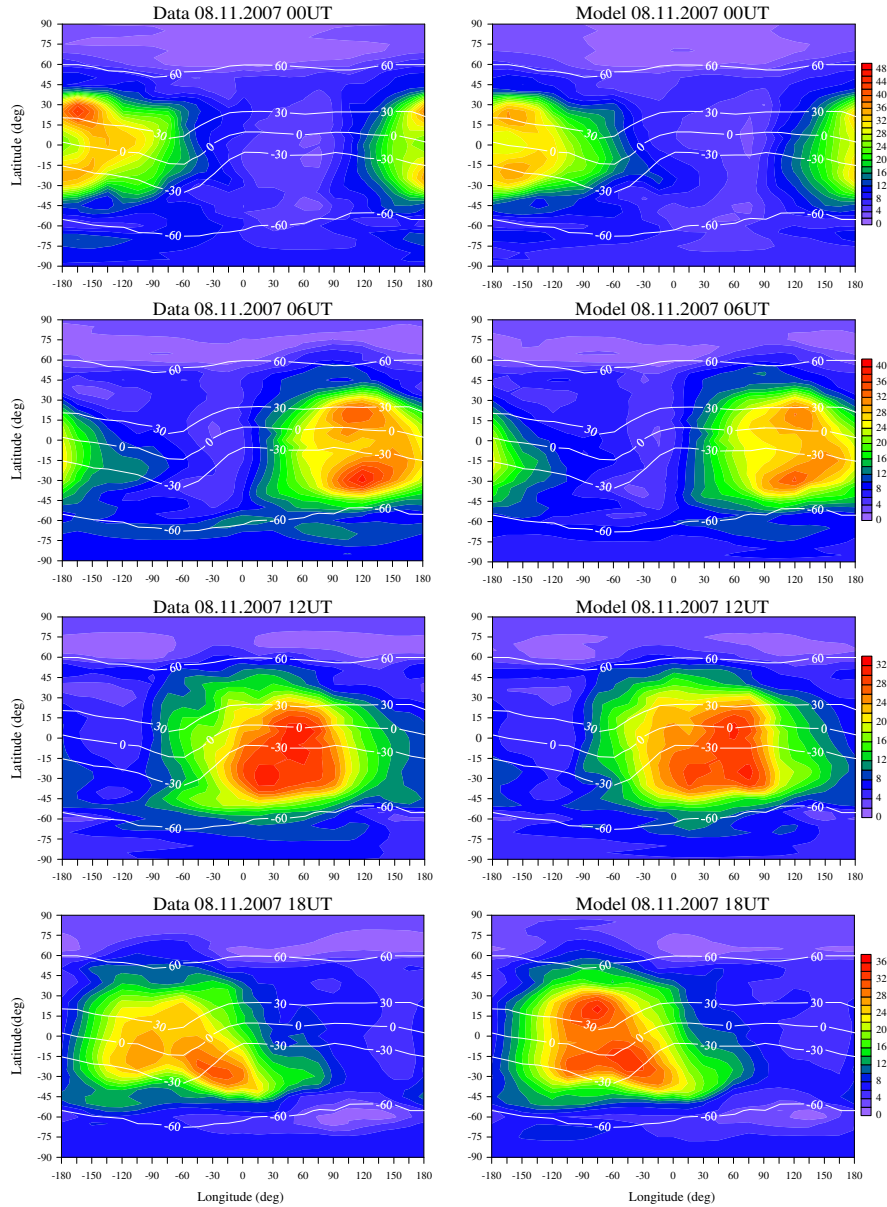


**Figure 11.** The same as Figure 10 but for 8 November 2007 quiet time day.

TEC maps (at one and the same UT) are the same. Due to the dependence of the TEC on the UT, the color scales are not the same at different UT. In general, there is significant similarity between the CODE and model TEC maps, but there are differences as well. At 00 UT and 06 UT, for example, the equatorial anomaly is underestimated by the model, but the hemispheric asymmetry is quite well reproduced. At 12 UT and 18 UT, the model's densest part of the ionosphere is closer to the observations; some longitude structures, as for example the WSA in the SH at 18 UT [He *et al.*, 2009; Chen *et al.*, 2011; Karpachev *et al.*, 2011], can be reproduced well. It is worth mentioning that the global background TEC model [Mukhtarov *et al.*, 2013a] constructed on the basis of the same CODE TEC data set is able to reproduce the well-known ionospheric structures as WSA and some longitudinal wave-like structures because it includes the effects of the nonmigrating tides and stationary planetary waves.

[42] The rTEC model response to the geomagnetic activity presented here can be used also when the geomagnetic activity is very low, i.e., during quiet geomagnetic conditions. Figure 11 shows a comparison between the model (right column) and CODE TEC maps for 8 November 2007 when the geomagnetic activity was very low, the daily averaged  $K_p$  index  $< 2$ . A general similarity between the model and CODE TEC maps is seen here as well. Again, the model crests of the equatorial ionization anomaly at 00 UT and 06 UT are slightly weaker than the observed ones, but the hemispheric asymmetry is well reproduced. The high degree of similarity is seen at 12 UT; at 18 UT the model TEC values are slightly larger than the observed ones.

[43] The above presented comparison between the model and CODE TEC maps revealed good similarity. This means that the global TEC model response to the geomagnetic activity constructed in this study could be used for both science and possible service (nowcasting and short-term prediction).

## 7. Summary

[44] In this study we present a global empirical TEC model response to geomagnetic activity described by the  $K_p$  index. The model is built on the basis of full 13 years (January 1999 to December 2011) of CODE TEC data. It describes the most probable spatial distribution and temporal variability of the geomagnetically forced TEC anomalies assuming that these anomalies at a given modip latitude depend mainly on the  $K_p$  index, LT, and longitude. The geomagnetic anomalies are expressed by the relative deviation of TEC from its 15 day median, noted as rTEC. Therefore, this model predicts the correction to the 15 day median values, rTEC, for each hour of the prediction period. The model offers TEC maps which depend on geographic coordinates ( $5^\circ \times 5^\circ$  in latitude and longitude) and UT at given geomagnetic activity and day of the year.

[45] The approach for building this model is based on the 2-D cross-correlation analysis between the rTEC and the geomagnetic  $K_p$  index. The existence of two types of the rTEC response, positive and negative, with different durations and time lags, has been found. An attempt for modeling the cross-correlation function between the rTEC and the geomagnetic  $K_p$  index has been made as well. The presence of two positive and negative rTEC responses to the geomagnetic activity imposed the implementation of two different time delay constants  $T_s$  and  $T_l$  in order to describe the two different delayed reactions. In this way the rTEC response to the geomagnetic activity is presented by a sum of two responses with different time delay constants and with different signs of the cross-correlation function. Based on these time constants, new modified functions of  $K_p$  index were defined, with variations closely resembling those of rTEC. It has been found that the mean dependence of rTEC on  $K_p$  index can be expressed by a cubic function. The LT dependence of rTEC is described by Fourier time series, which includes the contribution of four diurnal components with periods 24, 12, 8, and 6 h. The rTEC dependence on longitude is presented by Fourier series, which includes the contribution of zonal waves with zonal wave numbers up to 6. A separate model, described by 10, is constructed at each modip latitude. The rTEC model contains 820 constants, and they are determined by least squares fitting techniques. The global model is obtained by the interpolation procedure called Inverse Distance Method [Shepard, 1968]. The presented comparison between the model results and CODE TEC data for three geomagnetic storms at different solar cycle and seasonal conditions (Figures 6, 7, and 8) demonstrated comparatively high degree of similarity. The very small systematic error ( $-0.204$ ) and low RMSE (4.592 TECU) of the model, calculated on the basis of the entire data set, characterized it as useful tool for describing the ionospheric TEC response to geomagnetic storms.

[46] This model could be used also for service, i.e., for nowcasting and short-term prediction. For this purpose, however, a detailed validation of the model at different geophysical conditions has to be performed in order to clarify the model predicting quality. We have to note that the above demonstrated ability of the model to reproduce the spatial-temporal features of the TEC response to geomagnetic activity at different geophysical conditions does not mean a validation of the TEC model; it is applied to the data that have been used for generating the model. Figures 6b, 6c, 7b, 7c, 8b, and 8c display actually the quality assessment of

the constructing model procedure. If the validation of the model demonstrates good predicting ability, then at a given day of the year, geographical location, and UT, the model needs as input parameter only the predicted  $K_p$  index. This is a possible task because there are available models which predict the geomagnetic activity with a reliable accuracy. An example of such model is a MAK model described by Andonov *et al.* [2004]. This model provides online prediction of the  $K_p$  index and is implemented on the Web site [http://www.geophys.bas.bg/kp\\_for/kp\\_mod\\_bg.php](http://www.geophys.bas.bg/kp_for/kp_mod_bg.php). The short-term TEC prediction, particularly at strong geomagnetic storms, will improve significantly the accuracy of the geodetic and navigation data, which have increasing importance in resolving both scientific and practical tasks.

[47] **Acknowledgments.** We are grateful to the CODE TEC team for access to the TEC data provided from the CODE FTP directory: <ftp://ftp.unibe.ch/aiub/CODE/>. This work was supported by the European Office of Aerospace Research and Development (EOARD), Air Force Office of Scientific Research, Air Force Material Command, USAF, under grant FA8655-12-1-2057 to D. Pancheva. We thank the anonymous reviewers for their insightful comments on the original manuscript.

[48] Robert Lysak thanks Francisco Azpilicueta, Alan Burns, and an anonymous reviewer for their assistance in evaluating this paper.

## References

- Afraimovich, E., O. Lesyuta, I. Ushakov, and S. Voeykov (2009), Geomagnetic storms and the occurrence of phase slips in the reception of GPS signals, *Ann. Geophys.*, *45*(1), doi:10.4401/ag-3494.
- Andonov, B., P. Mukhtarov, and I. Kutiev (2004), Analogue model, relating  $K_p$  index to solar wind parameters, *J. Atmos. Sol. Terr. Phys.*, *66*, 927–932.
- Andonov, B., P. Mukhtarov, and D. Pancheva (2011), Empirical model of the TEC response to the geomagnetic activity over the North American region, *Adv. Space Res.*, *48*, 1041–1048, doi:10.1016/j.asr.2011.05.007.
- Araujo-Pradere, E. A., T. J. Fuller-Rowell, and P. S. J. Spencer (2006), Consistent features of TEC changes during ionospheric storms, *J. Atmos. Sol. Terr. Phys.*, *68*(16), 1834–1842.
- Azpilicueta, F., C. Brunini, and S. M. Radicella (2006), Global ionospheric maps from GPS observations using modip latitude, *Adv. Space Res.*, *38*, 2324–2331.
- Buonsanto, M. J. (1999), Ionospheric storms: A review, *Space Sci. Rev.*, *88*, 563–601.
- Chen, C. H., J. D. Huba, A. Saito, C. H. Lin, and J. Y. Liu (2011), Theoretical study of the ionospheric Weddell Sea Anomaly using SAMI2, *J. Geophys. Res.*, *116*, A04305, doi:10.1029/2010JA015573.
- Crowley, G., A. Reynolds, J. P. Thayer, J. Lei, L. J. Paxton, A. B. Christensen, Y. Zhang, R. R. Meier, and D. J. Strickland (2008), Periodic modulations in thermospheric composition by solar wind high speed streams, *Geophys. Res. Lett.*, *35*, L21106, doi:10.1029/2008GL035745.
- Dow, J. M., R. E. Neilan, and C. Rizos (2009), The International GNSS Service in a changing landscape of Global Navigation Satellite Systems, *J. Geod.*, *83*, 191–198, doi:10.1007/s00190-008-0300-3.
- Elmas, Z. G., M. Aquino, H. A. Marques, and J. F. G. Monico (2011), Higher order ionospheric effects in GNSS positioning in the European region, *Ann. Geophys.*, *29*, 1383–1399, doi:10.5194/angeo-29-1383-2011.
- Ercha, A., D. Zhang, A. J. Ridley, Z. Xiao, and Y. Hao (2012), A global model: Empirical orthogonal function analysis of total electron content 1999–2009 data, *J. Geophys. Res.*, *117*, A03328, doi:10.1029/2011JA017238.
- Feltens, J. (2007), Development of a new three-dimensional mathematical ionosphere model at European Space Agency/European Space Operations Centre, *Space Weather*, *5*, S12002, doi:10.1029/2006SW000294.
- Feltens, J., and S. Schaer (1998), IGS products for the ionosphere, in *IGS Position Paper, in IGS 1998 Analysis Center Workshop: Proceedings*, edited by J. M. Dow, J. Kouba, and T. Springer, pp. 225–232, Eur. Space Oper. Cent., Darmstadt, Germany.
- Field, P. R., and H. Rishbeth (1997), The response of the ionospheric  $F_2$ -layer to geomagnetic activity: An analysis of worldwide data, *J. Atmos. Sol. Terr. Phys.*, *59*, 163–180.
- Fuller-Rowell, T. J., M. V. Codrescu, R. J. Moffett, and S. Quegan (1994), Response of the thermosphere and ionosphere to geomagnetic storms, *J. Geophys. Res.*, *99*, 3893–3914.

- Fuller-Rowell, T. J., M. V. Codrescu, H. Rishbeth, R. J. Moffett, and S. Qegan (1996), On the seasonal response of the thermosphere and ionosphere to geomagnetic storms, *J. Geophys. Res.*, *101*, 2343–2353.
- Fuller-Rowell, T. J., M. V. Codrescu, and M. Wilkinson (2000), Quantitative modelling of the ionospheric response to geomagnetic activity, *Ann. Geophys.*, *18*, 766–781.
- Gao, Y., P. Heroux, and J. Kouba (1994), Estimation of GPS receiver and satellite L1/L2 signal delay biases using data from CACS, paper presented at the International Symposium on Kinematic Systems in Geodesy, Geomatics, and Navigation, Univ. of Calgary, Banff, Alberta, Canada.
- Ge, S., C. Shum, L. Potts, Y. Yi, T. Hobiger, H. Schuh, D. K. Bilitza, P. Callahan, J. Ping, and K. Matsumoto (2004), Comparison of TEC measurements from dual frequency space geodetic techniques, *Eos Trans. AGU*, *85*(47), Fall Meet. Suppl., Abstract G53A-0118.
- Habarulema, J. B., L.-A. Mc Kinnell, and P. J. Cilliers (2007), Prediction of GPS total electron content using neural network over South Africa, *J. Atmos. Sol. Terr. Phys.*, *69*(15), 1842–1850.
- Habarulema, J. B., L.-A. McKinnell, and B. D. L. Opperman (2010), TEC measurements and modelling over Southern Africa during magnetic storms; a comparative analysis, *J. Atmos. Sol. Terr. Phys.*, *72*, 509–520, doi:10.1016/j.jastp.2010.01.012.
- Habarulema, J. B., L.-A. McKinnell, and B. D. L. Opperman (2011), Regional GPS TEC modeling: Attempted spatial and temporal extrapolation of TEC using neural networks, *J. Geophys. Res.*, *116*, A04314, doi:10.1029/2010JA016269.
- He, M., L. Liu, W. Wan, B. Ning, B. Zhao, J. Wen, X. Yue, and H. Le (2009), A study of the Weddell Sea anomaly observed by FORMOSAT-3/COSMIC, *J. Geophys. Res.*, *114*, A12309, doi:10.1029/2009JA014175.
- Hernández-Pajares, M., J. M. Juan, and J. Sanz (1997), High-resolution TEC monitoring method using permanent ground GPS receivers, *Geophys. Res. Lett.*, *24*, 1643–1646, doi:10.1029/97GL01591.
- Hernández-Pajares, M., J. M. Juan, J. Sanz, R. Orus, A. Garcia-Rigo, J. Feltens, A. Komjathy, S. C. Schaer, and A. Krankowski (2009), The IGS VTEC maps: A reliable source of ionospheric information since 1998, *J. Geod.*, *83*, 263–275, doi:10.1007/s00190-008-0266-1.
- Ho, C. M., A. J. Mannucci, U. J. Lindqwister, X. Pi, and B. T. Tsurutani (1996), Global ionosphere perturbations monitored by the worldwide GPS network, *Geophys. Res. Lett.*, *23*, 3219–3222, doi:10.1029/96GL02763.
- Hoque, M. M., and N. Jakowski (2007), Higher order ionospheric effects in precise GNSS positioning, *J. Geod.*, *81*(4), 259–268, doi:10.1007/s00190-006-0106-0.
- Jakowski, N., S. M. Stankov, and D. Klaehn (2005), Operational space weather service for GNSS precise positioning, *Ann. Geophys.*, *23*(9), 3071–3079.
- Jee, G., H.-B. Lee, Y. H. Kim, J.-K. Chung, and J. Cho (2010), Assessment of GPS global ionosphere maps (GIM) by comparison between CODE GIM and TOPEX/Jason TEC data: Ionospheric perspective, *J. Geophys. Res.*, *115*, A10319, doi:10.1029/2010JA015432.
- Karpachev, A. T., N. A. Gasilov, and O. A. Karpachev (2011), Morphology and causes of the Weddell Sea anomaly, *Geomagn. Aeron.*, *51*(6), 812–824, doi:10.1134/S0016793211050070.
- Kashcheyev, A., B. Nava, and S. M. Radicella (2012), Estimation of higher-order ionospheric errors in GNSS positioning using a realistic 3-D electron density model, *Radio Sci.*, *47*, RS4008, doi:10.1029/2011RS004976.
- Kutiev, I., and P. Muhtarov (2001), Modeling of midlatitude  $F$  region response to geomagnetic activity, *J. Geophys. Res.*, *106*, 15,501–15,510.
- Kutiev, I., and P. Muhtarov (2003), Empirical modeling of global ionospheric  $f_oF_2$  response to geomagnetic activity, *J. Geophys. Res.*, *108*(A1), 1021, doi:10.1029/2001JA009134.
- Mendillo, M. (1973), A study of the relationship between geomagnetic storms and ionospheric disturbances at mid-latitudes, *Planet. Space Sci.*, *21*, 349–358.
- Mendillo, M. (2006), Storms in the ionosphere: Patterns and processes for total electron content, *Rev. Geophys.*, *44*, RG4001, doi:10.1029/2005RG000193.
- Mendillo, M., M. D. Papagiannis, and J. A. Klobuchar (1970), Ionospheric storms at midlatitudes, *Radio Sci.*, *5*, 895–898.
- Mendillo, M., J. A. Klobuchar, and H. Hajeb-Hosseini (1974), Ionospheric disturbances: Evidence for the contraction of the plasmasphere during severe geomagnetic storms, *Planet. Space Sci.*, *22*, 223–236.
- Mendillo, M., X.-Q. He, and H. Rishbeth (1992), How the effects of winds and electric fields in  $F_2$ -layer storms vary with latitude and longitude: A theoretical study, *Planet. Space Sci.*, *40*, 595–606.
- Mikhailov, A., and K. Schlegel (1998), Physical mechanism of strong negative storm effects in the daytime ionospheric  $F_2$  region observed with EISCAT, *Ann. Geophys.*, *16*, 602–608.
- Muhtarov, P., and I. Kutiev (1998), Empirical modeling of ionospheric storms at midlatitudes, *Adv. Space Res.*, *22*(6), 829–832.
- Muhtarov, P., I. Kutiev, and L. Cander (2002), Geomagnetically correlated autoregression model for short-term prediction of ionospheric parameters, *Inverse Probl.*, *18*, 49–65.
- Mukhtarov, P., and D. Pancheva (2011), Global ionospheric response to nonmigrating DE3 and DE2 tides forced from below, *J. Geophys. Res.*, *116*, A05323, doi:10.1029/2010JA016099.
- Mukhtarov, P., and D. Pancheva (2012), Thermosphere–ionosphere coupling in response to recurrent geomagnetic activity, *J. Atmos. Sol. Terr. Phys.*, *90*, 132–145.
- Mukhtarov, P., D. Pancheva, B. Andonov, and L. Pashova (2013a), Global TEC maps based on the GNSS data: 1. Empirical background TEC model, *J. Geophys. Res. Space Physics*, *118*, 4594–4608, doi:10.1002/jgra.50413.
- Mukhtarov, P., D. Pancheva, B. Andonov, and L. Pashova (2013b), Global TEC maps based on the GNSS data: 2. Model evaluation, *J. Geophys. Res. Space Physics*, *118*, 4594–4608, doi:10.1002/jgra.50412.
- Pröls, G. W. (1980), Magnetic storm associated perturbations of the upper atmosphere: Recent results obtained with satellite-borne gas analyzers, *Rev. Geophys.*, *18*, 183–202.
- Pröls, G. W. (1991), Thermosphere-ionosphere coupling during disturbed conditions, *J. Geomagn. Geoelectr.*, *43*(suppl.), 537–549.
- Pröls, G. W. (1993), On explaining the local time variations of ionospheric storm effects, *Ann. Geophys.*, *11*, 1–9.
- Pröls, G. W. (1995), Ionospheric  $F$  region storms, in *Handbook for Atmospheric Electrodynamics*, vol. 2, edited by H. Volland, pp. 195–248, CRC Press, Boca Raton.
- Pröls, G. W. (2005), Space weather effects in the upper atmosphere: Low and middle latitudes, in *Space Weather*, Lecture Notes in Physics, vol. 656, edited by K. Scherer et al., pp. 193–234, Springer, Berlin.
- Pröls, G. W. (2008), Ionospheric storms at mid-latitudes: A short review, in *Midlatitude Ionospheric Dynamics and Disturbances*, AGU Monograph, vol. 181, edited by P. M. Kintner, pp. 9–24, AGU, Washington, D. C.
- Pröls, G. W. (2011), Density perturbations in the upper atmosphere caused by the dissipation of solar wind energy, *Surv. Geophys.*, *32*(2), 101–195.
- Rawer, K. (1963), Propagation of decimeter waves (HF-band), in *Meteorological and Astronomical Influences on Radio Wave Propagation*, edited by B. Landmark, pp. 221–250, Pergamon Press, Oxford.
- Rawer, K. (Ed) (1984), *Encyclopedia of Physics*, Geophysics III, Part VII, vol. 49, pp. 389–391, Springer-Verlag, New York.
- Rishbeth, H. (1991),  $F$  region storms and thermospheric dynamics, *J. Geomagn. Geoelectr.*, *43*(suppl.), 513–524.
- Rishbeth, H. (1998), How the thermospheric circulation affects the ionospheric  $F_2$ -layer, *J. Atmos. Terr. Phys.*, *60*, 1385–1402.
- Schaer, S. (1999), Mapping and predicting the Earth's ionosphere using the Global Positioning System, *Geod. Geophys. Arb. Schweiz.*, vol. 59, Inst. für Geod. und Photogram., Zurich, Switzerland.
- Shepard, D. (1968), A two-dimensional interpolation function for irregularly-spaced data, *ACM '68 Proc.*, pp. 517–524, ACM New York, NY, doi:10.1145/800186.810616.
- Sojka, J., R. L. McPherron, A. P. van Eyken, M. J. Nicolls, C. J. Heinselman, and J. D. Kelly (2009), Observations of ionospheric heating during the passage of solar coronal hole fast streams, *Geophys. Res. Lett.*, *36*, L19105, doi:10.1029/2009GL039064.
- Stankov, S. M., I. Kutiev, N. Jakowski, and A. Wehrenpfennig (2001), A new method for total electron content forecasting using global positioning system measurements, *Proc. ESTEC Workshop on Space Weather*, 17–19 Dec. 2001, Noordwijk, The Netherlands, 169–172.
- Stankov, S. M., I. S. Kutiev, N. Jakowski, and A. Wehrenpfennig (2004), GPS TEC forecasting based on auto-correlation analysis, *Acta Geod. Geophys. Hung.*, *39*(1), 1–14.
- Stankov, S. M., K. Stegen, and R. Warnant (2010), Seasonal variations of storm-time TEC at European middle latitudes, *Adv. Space Res.*, *46*(10), 1318–1325.
- Tanaka, T. (1979), The worldwide distribution of positive ionospheric storms, *J. Atmos. Terr. Phys.*, *41*, 103–110.
- Tanaka, T. (1981), Severe ionospheric disturbances caused by the sudden response of evening subequatorial ionospheres to geomagnetic storms, *J. Geophys. Res.*, *86*, 11,335–11,349.
- Wang, X., Q. Sun, R. Eastes, B. Reinisch, and C. E. Valladares (2008), Short-term relationship of total electron content with geomagnetic activity in equatorial regions, *J. Geophys. Res.*, *113*, A11308, doi:10.1029/2007JA012960.
- Zhao, B., W. Wan, L. Liu, and T. Mao (2007), Morphology in the total electron content under geomagnetic disturbed conditions: Results from global ionosphere maps, *Ann. Geophys.*, *25*, 1555–1568, doi:10.5194/angeo-25-1555-2007.